Characterization and evaluation of commercial biochar for surface water purification

Sustainable Horizons 15 (2025) 100145

Contents lists available at ScienceDirect

Sustainable Horizons

journal homepage: www.elsevier.com/locate/horiz

Original Research Articles

Characterization and evaluation of commercial biochar for surface water purification

Lorenzo Animali [a,*], Sveva Corrado [a], Nicola Mitillo [a], Paola Tuccimei [a], Mattia Bartoli [b], Massimo Mattei [a], Mauro Giorcelli [b]

[a] Department of Science, Geology Section, Roma Tre University, L. go S. Leonardo Murialdo 1, 00146 Rome, Italy
[b] Department of Applied Science and Technology, Politecnico di Torino, C.so Duca degli Abruzzi 24, 10129 Turin, Italy

ARTICLE INFO

Keywords:
Biochar
Water pollution
Heavy metals
Carbon storage
Italy
SDGs 6, 11, 13

ABSTRACT

Biochar is a promising material for carbon storage and water purification, particularly for heavy metal removal. The transition from laboratory studies to real-world applications remains challenging due to variability in commercial biochar properties and lack of testing on multi-contaminant matrixes.

The study aims at bridging such a gap by characterizing and testing nine commercial biochar in the real case scenario of the area surrounding the decommissioned Malagrotta landfilling site (Latium region, central Italy). The area is notorious for legal, social, health and environmental issues. Periodic monitoring performed by local authorities classifies chemical water quality as scarce. In this context, the effect of environmental water-biochar interactions was tested on surface water samples. Biochar multi-method characterization was carried out through optical microscopy, SEM, EDX spectroscopy, X-ray diffraction, ICP-MS, pH-electric conductivity and FT-IR spectroscopy.

Biochar characterization allowed systematic comparison not possible trough commercial labels: bulk composition is carbonaceous (78–92 %); mineralization mostly consists of calcite (<8 % for most samples); heavy metal contaminants are present (up to >100 ppm for Chromium and Zinc); pH ranges from 8 to 12, bearing exponential relationship with electrical conductivity (EC230–2417 μS); FT-IR spectra testify high aromaticity and variability in oxygenated (≈1700 cm^{-1}) functional groups, less abundant in pyro-gasification-produced biochar compared to pyrolysis-produced ones.Contrary to expectations, trace pollutant concentrations in Malagrotta waters are within legal limits. Thus Malagrotta case study explores bottom thresholds for surface water treatment using biochar. Low trace contaminant concentrations hinder detection of adsorption phenomena. Moreover, leaching tests utilising drinking water and high biochar dosage (10 g/L) demonstrate biochar's safety, as leaching is limited to few μg/L. These results are instrumental in elaborating biochar specific water treatment regulations.

1. Introduction

Biochar is defined by the European Biochar Certificate (EBC) as a “porous, carbonaceous material that is produced by pyrolysis of biomass and is applied in such a way that the contained carbon remains stored as a long-term C sink or replaces fossil carbon in industrial manufacturing. It is not made to be burnt for energy generation” (EBC, 2023). Accordingly, pyrolysis can be identified as the main process of thermal decomposition of biomass in oxygen limited conditions (Adhikari et al., 2018; Brassard et al., 2017; Kersten and Garcia-Perez, 2013; Kwon et al., 2019; Weber and Quicker, 2018), but an unambiguous definition has not yet been established. Indeed, several associations, research institutes and policy makers set different constraints on what can be defined as biochar. These constraints mostly depend on the feedstock type and the production process (Lehmann et al., 2021; Oni et al., 2019; Pourhashem et al., 2019; Sakhiya et al., 2020; Wang and Wang, 2019; Xiao et al., 2018).

The potential of biochar as an adsorbent material rises from its similarity to activated carbon (Castiglioni et al., 2022; Inyang et al., 2016; Tan et al., 2017). Crucial properties in this regard include a high surface area and presence of adequate surface functional groups (Inyang and Dickenson, 2015; Weber and Quicker, 2018; Wei et al., 2018). The former allows greater surface for interaction. The latter improves the ability of biochar to bind specific pollutants (Dai et al., 2021; Liu et al.,

* Corresponding author.
E-mail address: lorenzo.animali@uniroma3.it (L. Animali).

https://doi.org/10.1016/j.horiz.2025.100145
Received 20 December 2024; Received in revised form 19 March 2025; Accepted 27 March 2025
Available online 28 April 2025

2019; Zhao et al., 2021). Such characteristics have sparked research concerning removal from synthetic solutions (Wang et al., 2020; Yu et al., 2024). Nevertheless, synthetic solutions do not accurately represent real world waters needing treatment (Chen et al., 2022; Kamali et al., 2021). Employed biochar tends to be laboratory-made and is not widely available (Alsawy et al., 2022). However, availability is a crucial factor for extensive adoption of innovative materials such as biochar. As a consequence, it should be considered in transitioning from novelty to viable application, such as water pollution remediation (Alsawy et al., 2022; Chen et al., 2019; Nair et al., 2017; Pourhashem et al., 2019).

Water pollution is among the global challenges to be addressed, as water constitutes a key resource for humanity's sustenance and development (Joshi et al., 2022; Wheater and Gober, 2015; Zamora-Ledezma et al., 2021). Moreover, freshwater use has experienced continuous growth, annually increasing by 1 % since 1980, highlighting its crucial role for a wide range of applications (UNESCO, 2021). Water pollution sources are mainly concentrated in areas characterized by urbanization, industrialization and agricultural activities (Lin et al., 2022; Morin-Crini et al., 2022; Schwarzenbach et al., 2010). Current research testifies that untreated wastewater accounts for 50 %, making urban areas a priority for intervention (Jones et al., 2022; Joshi et al., 2022; Strokal et al., 2021). There is consensus about the potential of biochar as an adsorbent material. However, this consensus largely stems from experiments that are not fully representative of real-world conditions. This work seeks to begin bridging the gap between research and practical application by using commercial biochar in a real-world case study. This can be a

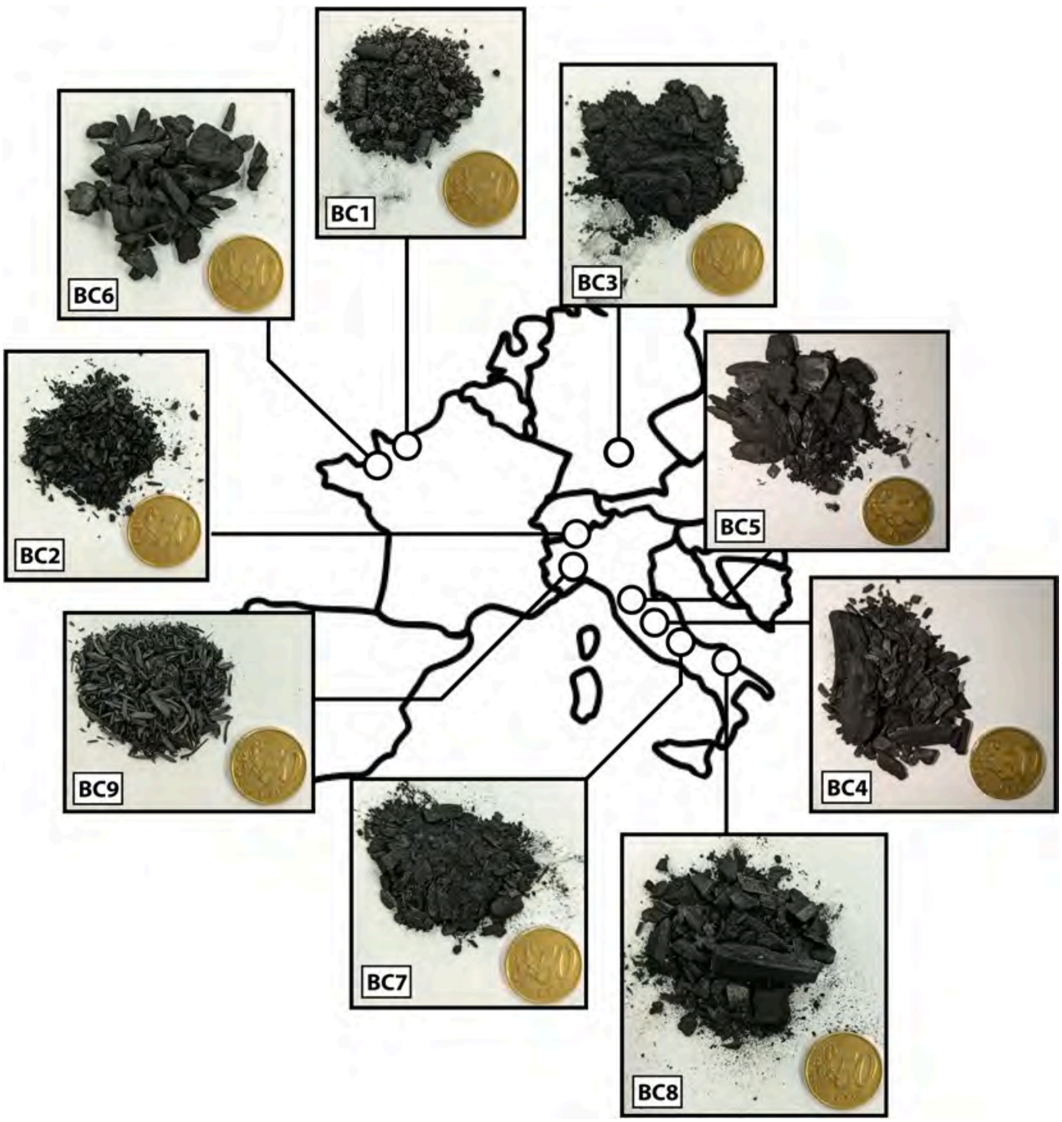

Fig. 1. Macroscopic images of biochar samples and related production locations. **BC1 -** Homogeneous material split between two main granulometries. The coarse one is constituted by cylindric pellets 5–20 mm in length and 4–5 mm of diameter. The finer fraction is constituted by fragmented pellets. Material is dry and frees ashes. **BC2 -** Homogeneous material in fine gravel range, made up of a mixture of elongated, splinter like, particles and irregular grains. The material is humid and does not free ashes. **BC3 -** Fine homogeneous material (fine sand grain-size, single grains can be distinguished by naked eye). Centimetric fragments are also present within the fine material. The material is dry, ashes are present. **BC4 -** Heterogeneous material made up of millimetric to centimetric size fragments, dry, does not free ashes. Original wood chip shape is preserved. **BC5 -** Very heterogeneous material made up of sub-millimetric to centimetric size fragments, dry, frees little ashes. Original wood chip shape is preserved in the coarser fraction. **BC6 -** Rather homogeneous material, made up of centimetric to millimetric size fragments, dry, frees little ashes. Original wood chip shape is preserved. **BC7 -** Very heterogeneous material made up of sub-millimetric to centimetric fragments immersed within very fine-grained groundmass, dry, frees large amounts of ashes. Original wood chip shape is preserved in the coarser portion of the material. **BC8 -** Very heterogeneous material made up of sub-millimetric to centimetric fragments; very fine-grained groundmass is present as well dry, frees ashes. Original wood chip shape is preserved in coarser portion of the material. **BC9 -** Very homogeneous material made up of elongated millimetric size fragments. Dry, does not free ashes. Original rice husk shape is preserved.

starting point for future research across different scenarios. Moreover, no biochar specific regulation for water treatment exists up to now. However, any material employed for this purpose in Europe would need to comply with the regulation concerning registration, evaluation, authorisation and restriction of chemicals (REACH) 1907/2006/EC and with the water framework directive 2000/60/EC (EU, 2000; 2006).

The materials used are nine commercial biochar from Italy and Europe. All of them are readily available for bulk purchase. Their accessibility enables immediate large-scale and real-world applications. The approach is twofold, focusing on both biochar characterization and the environmental case study. Routine and innovative techniques are used to characterise and effectively compare samples to identify the most relevant properties for the given application.

A sampling in the area surrounding the decommissioned Malagrotta landfill has been conducted to assess surface water quality. The area has historically been source of concern for local authorities due to improper management practices (Barbieri et al., 2014; Daniele and Fabiani, 2020). Biochar adsorption tests were performed on the sampled surface waters. Results testify pollutant concentrations in the adsorbent being greater than in the matrix, thus hindering detection of absorption phenomena. This provided local authorities with evidence to assess surface water quality in the area. Furthermore, pollutant leaching tests from biochar have been performed to ensure safety of biochar use. The leaching from biochar is limited to few µg/L constituting no risk to human health and the environment.

2. Materials and methods

2.1. Materials

This study started from scratch to test the challenges posed by the potential implementation of a biochar-based solution for water purification in a real-world scenario. Nine commercial biochar types were collected focusing on the national market, but also including European counterparts for the sake of comparison (Fig. 1).

"Commercial biochar" is hereby defined as a material that is currently available in bulk (either through direct purchase of the product or through agreements with the producers) and in large quantity thus allowing easy scale-up. Six out of nine biochar are produced in Italy (BC2, BC4, BC5, BC7, BC8, BC9). Two come from France (BC1, BC6) and one from Germany (BC3). In Tables 1 and 2, we provide a concise macroscopic description of biochar, the availability of information derived by official labels accompanying the product, in agreement with law restrictions of the production countries (D. Lgs., 2023 for Italy). Regarding the production process, BC1, BC2, BC5, BC6, BC9 are declared as produced by pyrolysis alone, BC3 and BC7 by pyro-gasification, whereas for BC4 and BC8 no certification on the process is available.

Moreover, pieces of information reported in Table 2 are not homogeneous, as the European biochar certificate (EBC, 2023) is currently still a voluntary EU standard, despite being one of the best efforts to standardize biochar characterization and provide guidance for customers and policy makers. Producers can employ it to differentiate their products, but currently, it is only mandatory in Switzerland for biochar intended for agricultural use. Other standards do exist (Amin et al., 2016; Leng et al., 2019; Meyer et al., 2017). However, the term biochar does not yet have a precise definition. Thus, the composition and production process of the so-called biochar are not yet well constrained (Rajput et al., 2024; Sakhiya et al., 2020; Weber and Quicker, 2018). As a result, biochar characteristics are also tied to local regulations. Italian policymakers have included biochar as a viable mean of soil amendment, through a modification of D. Lgs.75/2010 in 2015, which allows only feedstocks of plant origin (D. Lgs., 2010). A similar criterion was used by the European Commission in its executive regulation EU 2019/2164, allowing biochar for organic agriculture (EU, 2019). Nevertheless, the EBC does not constrain feedstock nature, but refers generically to an origin from "biomass". On the other hand, use cases are specified (EBC, 2023). Therefore, the term "biochar" comes out as

Table 1
Main features of the nine commercial biochar employed in this work (in green, when present): production country, feedstock, production process and qualitative description. The description relates to bulk material straight out of its packaging. Grain size is defined as: fine (sub-millimetric); medium (millimetric to centimetric); coarse (centimetric only). For the sake of simplicity and need of anonymity, commercial names are omitted, and biochar are labelled by progressively numbered acronyms. Humidity is to be intended as perceived through touch. Ashes are to be intended as amount of dust being freed while handling the material.

	ORIGIN			DESCRIPTION				
Sample	**Production country**	**Feedstock**	**Production Process**	**Fine**	**Medium**	**Coarse**	**Humidity**	**Ash**
BC1	France	Wood	Pyrolysis		✓			✓
BC2	Italy	Mix (IT law)	Pyrolysis		✓		✓	
BC3	Germany	Wood	Pyro-Gasification	✓		✓		✓
BC4	Italy	Mix (IT law)	Pyrolysis		✓	✓		
BC5	Italy	Poplar Wood	Pyrolysis	✓	✓	✓	✓	✓
BC6	France	Wood	Pyrolysis			✓		✓
BC7	Italy	Mix (IT law)	Pyro-Gasification	✓	✓	✓		✓
BC8	Italy	Mix (IT law)	Pyrolysis	✓	✓	✓		✓
BC9	Italy	Rice Husk	Pyrolysis		✓			

Table 2
Available trade label data (in green, when present): water retention, total humidity, total organic carbon (TOC), ash content, salinity, pH, nitrogen content (N), potassium content (as oxide, K_2O), phosphorus content (as oxide, P_2O_5) calcium content (as oxide, CaO), magnesium content (as oxide, MgO) sodium content (as oxide, Na_2O), hydrogen over carbon ratio (H/C). BC6 and BC9 are pre-distribution samples (not yet on the market). Please note the data are given as on the label.

Sample	Water retention [%]	Total Humidity [%]	TOC [%]	Ash content [%]	Salinity	pH	N [mg/kg]	K_2O [mg/kg]	P_2O_5 [mg/kg]	CaO [mg/kg]	MgO [mg/kg]	Na_2O [mg/kg]	H/C molar ratio
BC1			84				4000	6000	1000				
BC2	62	> 10	> 75	3.39	514 [meq/100g]	9.8	3990	848	294	3685	1007	49.4	0.07
BC3													
BC4	150	< 20	65	5.5	1.1 [dS/m]	9.85	< 5000	3020	340	9920	852	291	0.2
BC5		2.3	86	8		8	3000	4965		23142	2571	321	0.28
BC6													
BC7	400	20	68.4	6.4	5 [dS/m]	11.3	5000	4000	3000	11000	2000	2000	0.48
BC8			> 75				3000	848	294	3685	1007	49.4	
BC9													

loosely defined and unreliable when trying to point out a material with a specific set of properties. Standardization efforts are trying to put an end to such an ambiguity. However, their implementation in regulatory schemes is still uncomplete.

2.2. Methods

The following workflow consists of a two-pronged approach based on biochar characterization and application to the case study of surface water in the area of the Malagrotta landfill. The collected material is characterized through a series of routine and novel techniques. Moreover, the case study was selected in collaboration with local authorities to address possible relevant issues in the Roman urban context.

2.2.1. Biochar analysis

For organic petrography, biochar samples were quartered and a representative powder for each of them was mounted in epoxy resin and polished according to standard procedures (Bustin et al., 1985). Observation on polished surfaces were performed on randomly oriented grains using a Zeiss Axioskop 40 microscope, under oil immersion in reflected monochromatic non-polarized light (Tungsten-halogen Lamp 12 V, 100 W), connected with an Axiocam 105 color camera. Single fragments were described on the base of the classification proposed for the first time by Lester et al. (2010) and modified by Mastalerz et al. (2023).

Morphology of each sample has been surveyed through scanning electron microscopy (FE-SEM, Zeiss SupraTM 40). An energy dispersive X-Ray detector (EDX, Oxford Inca Energy 450) fitted on the microscope further allowed evaluation of biochar's elemental composition. EDX investigation for each sample is referred to area scanning (50 × 50 μm). Analysis must be considered as roughly representative of biochar composition as referred to a limited number of analysed areas for each sample.

X-ray diffraction analysis (XRD) has been employed to describe biochar's mineralogy. Biochar powder for each sample was examined trough a Bruker D8 Advance X-ray system with a Lynxeye XE-T silicon-strip detector at the Department of Earth Sciences, Sapienza University of Rome. Operation happened at 40 kV and 30 mA with CuKα radiation ($\lambda = 1.5406$ Å). Samples were scanned between 2 and 70° 2θ with step sizes of 0.02° 2θ.

Ion coupled plasma mass spectroscopy (ICP-MS) has been performed to determine elemental composition of biochar samples which have been pulverized (Activation Laboratories code RX4) (A. L. Ltd., 2024a) and analysed according to Ultratrace 4, near total digestion procedure (A. L. Ltd., 2024b).

PH and electric conductivity values have been measured through a multiparametric probe (Hanna instruments - multi-parameter pH/ORP/EC/Pressure/Temperature watertight meter - HI98195), according to the procedure described by Singh et al. (2017).

Fourier transform infrared spectroscopy (FT-IR) was applied to identify the functional groups on the different collected biochar. Bulk samples were prepared using the common KBr pellet method, widely used for coals characterization (Adhikari et al., 2024; Painter et al., 1981; Petersen et al., 2008). Biochar and KBr mixture at an approximately 1:100 ratio was used in pellet preparation and dried for 62 h at 105–110 °C in oven. A Nicolet iS50 spectrometer equipped with a DTGS detector was used for spectra acquisition. Absorption spectra were collected in a range between 500 and 4000 cm^{-1} averaging 64 scans with a resolution of 2 cm^{-1}. The raw FT-IR spectra data was initially processed to reduce noise with common preprocessing steps: baseline correction and normalization. From FT-IR spectra, the bands assignments of functional groups and semiquantitative data analysis were based on Painter et al., 1981, Lis et al., 2005, Petersen et al., 2008, Chen et al., 2008, Keiluweit et al., 2010, Chen et al., 2012, Singh et al., 2016, Zhang et al., 2020, Phan et al., 2021, Mastalerz et al., 2023, Adhikari et al., 2024.

2.2.2. Identification of the site and sampling procedure

The case study is the area surrounding the Malagrotta landfilling site in Rome municipality in the Lazio region (central Italy, Fig. 2). This area has historically been under special attention due to suspect inappropriate management practices and influx of large quantities of waste (Daniele and Fabiani, 2020). Closure of the landfilling site took place in 2013, but remediation works are still ongoing (ERAS, 2013).

The Malagrotta Landfilling site and the surrounding area, located in Rome municipality, have been object of interest since its opening in 1970 after which it quickly became Lazio's waste main destination (Barbieri et al., 2014). Its long operation period is characterized by allegations of improper disposal practices, alongside with public pressure due to environmental concern, up until closure in 2013 (Daniele and Fabiani, 2020). Despite the main activity having ceased, there are lingering issues still needing to be addressed. In fact, the presence of a landfilling site has created a significant socio-economic gap with respect to the surrounding areas while operations tide to waste processing have increased risk for respiratory, cardiovascular and tumoral illnesses (ERAS, 2013). On the legal side, the matter of cost subsidization for remediation operations is still open. Finally, the surrounding

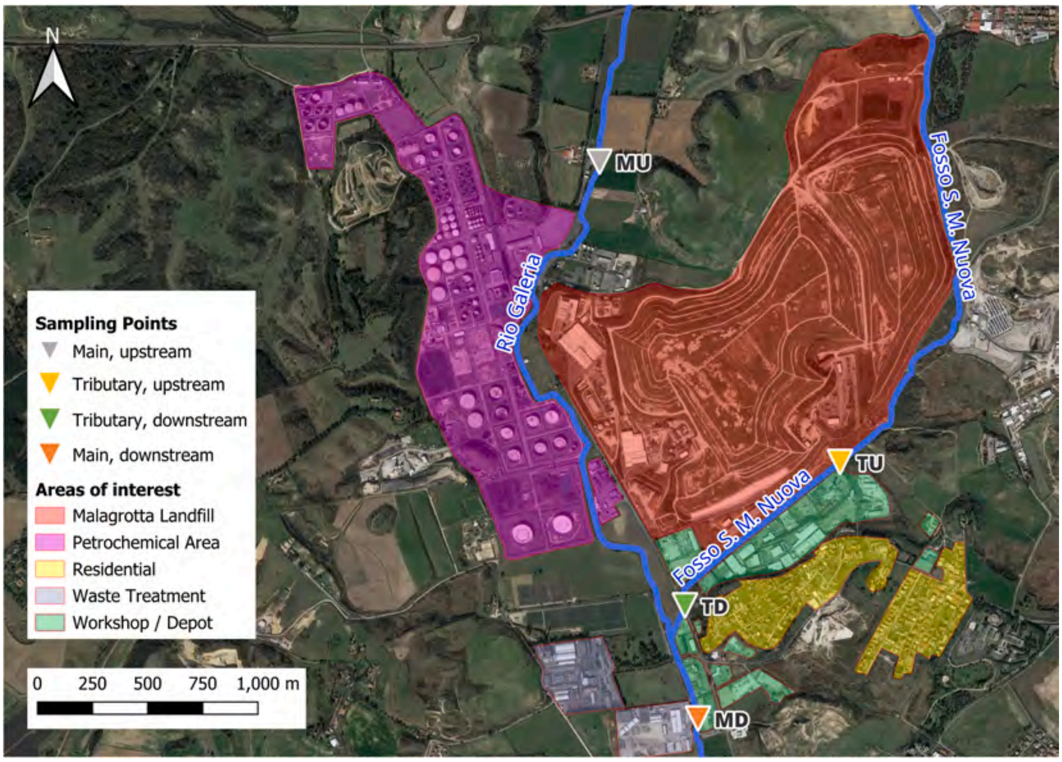

Fig. 2. Map of the study area, comprising of the former Malagrotta landfill and its surroundings. Waterways, areas of interest and sampling points are highlighted (QGIS, 2024; modified from Google Satellite).

environment has been altered by leaching of pollutants which caused toxic effects on fauna, flora homogenization and soil pollution from multiple contaminants, including heavy metals (Baderna et al., 2011; Filibeck et al., 2016). Other than the landfilling site, where remediation works are still going on, the area also hosts a petrochemical site and heavy-duty workshops (Fig. 2).

The case study for an attempt to apply biochar for surface water purification was identified with the help of the local authorities (Direzione Ambiente, Regione Lazio). This was done both to raise awareness about biochar's potential and to promote collaboration between academia and public institutions. The area surrounding the decommissioned Malagrotta landfill is currently devoted to industrial use. The hydrographic network consists of a main river and a tributary stream, Rio Galeria and Fosso Santa Maria Nuova respectively (Fig. 2). The main river is north-south oriented in the centre of the study area, roughly dividing it in two halves (Fig. 2). The tributary flows from the north to south in the eastern portion of the study area, then bends to the south-west before joining the main river (Fig. 2).

The Malagrotta landfill occupies most of the eastern portion of the study area lying between the main river and the tributary stream. In addition to the landfill, the area also hosts a large petrochemical plant in its western portion, along the main river right bank (Fig. 2). The south-eastern part is home to several mechanical workshops and depots as well as two residential areas, it is to the south of the tributary stream, on its hydrographic left bank. In the southernmost part of the study area, two water treatment facilities are located (Fig. 2). They occur to the south of the confluence of tributary and the main river and on the right bank with respect to the latter (Fig. 2). The remaining part of the study area is mostly occupied by agricultural land (Fig. 2).

Sampling was carried out in four sites that have potential for future on site biochar application, as accessibility and adequate flow rate are key features (Fig. 2). Sampling point Main Upstream (MU) is located in the northern part of the study area, uphill with respect to the hypothesized inflow influenced by the landfill and petrochemical area (Fig. 2). The TU sampling point lies uphill of the mechanical workshops to the south-east to monitor their influence on water quality (Fig. 2). The TD sampling point serves a similar purpose acting as a control, just before the confluence within the main river (Fig. 2). Sampling point MD is in the south of the study area, downstream the confluence (Fig. 2). This sampling point is employed to survey surface water outflow from the study area. It is also used by local authorities for periodic water quality assessment (ARPALAZIO, 2020). Publicly accessible results provide qualitative water quality evaluations for chemical and biological pollution. At the time of writing both parameters were unsatisfactory (ARPALAZIO, 2020). By sampling we wanted to assess pollutant pathways in the surface water in the area. With results coming from water chemical analysis, we were able to frame the context in terms of chemical pollution.

2.2.3. *Water analyses*

Water samples collected during the sampling survey and from laboratory experiments were analysed according to the following standard procedures:

- U.S. EPA 200.7 2001 for Sb, As, Be, Cd, Co, Cr, Ni, Pb, Cu, Se, Tl, V, Zn, Ca, Mg, Na, K (EPA, 1994).
- UNI EN ISO 12,846:2013 for Hg (ISO, 2012).
- UNI EN ISO 17,294–2:2023 for Zr, La (ISO, 2023).
- UNI EN ISO 10,304–1:2009 for sulphates, nitrates, phosphates, chlorides, fluorides (ISO, 2007).
- APAT CNR IRSA 4050 Man. 29 2003 for nitrites (APAT, 2003).
- U.S. EPA 9010C 2004 and EPA 9014 2014 for cyanides (EPA, 2014, 2004).

2.2.4. *Effect of biochar exposure to environmental water*

The first experiment was performed directly on sampled surface waters from the Malagrotta landfill area. The objective was to survey the feasibility of on-site biochar application. Employed water has been collected in correspondence of sampling point MU. This sampling point represents the convergence of the main and tributary stream and is also an historical sampling point for surface water surveys conducted by local environmental protection agencies (SIRA, 2024). Flow rate at the time of collection was also deemed appropriate for potential future on site experiments.

1 L of river water has been mixed with 10 g of biochar BC1 trough BC9 with particle size < 2 mm. Adsorption time at room temperature has been set to 7 days to simulate a real case scenario of biochar application. At the end of the experiment morphological changes on biochar's surface have been evaluated through SEM imagery.

2.2.5. *Contaminant leaching from biochar*

The matrix of choice for the experiment is store-bought mineral water. This experiment has been performed to test leaching of pollutants from biochar into clean, potable water. 200 ml of mineral water have been mixed with 2 g of biochar BC1 trough BC9 with particle size <2 mm. Adsorption time at room temperature has been set to 24 h as this time span encloses the period of greatest interaction between biochar and its surroundings. After this period water was centrifuged at 3000 rpm for 5 min (ALC PK120 centrifuge, Thermofisher scientific, Waltham, Massachusetts) and filtered through both 8 µm filter paper (Whatman® qualitative filter paper, Grade 2) and 0.45 µm membrane filters (Corning® syringe filters PTFE membrane, diam. 25 mm, pore size 0.45 µm) to remove solid residues. Analysis was then performed to determine occurrence and entity of leaching.

3. Results

3.1. *Biochar characterization*

In this paragraph main optical and SEM features for the nine analysed biochar are described. Representative images for each biochar sample are provided in Figs. 3 and 4.

BC1 (Figs. 3A and 4A) - Sample BC1 displays well preserved, frequently obliquely cut, plant tissue structures, with a predominance of cellular porosity over non-cellular porosity. The porosity is related to single cell lumens, separated by thick cell walls. No fractures interfere with the original structure of the wood and no cell collapse is observed. The fragments show a regular pore distribution, and no pore occlusion is detected. High reflectance inertinite is dominant, fusinite is prevalent and the mineral content is low. BC1 is homogeneous and can be predominantly placed in the inertoid category with >75 % unfused material. SEM images of BC1 show a rough surface highlighting internal planar structures. Smaller fragments adhere to external surfaces. No fractures or signs of alteration are observed.

BC2 (Figs. 3B and 4B) - Optical microscopy Images of sample BC2 show well-preserved cell wall margins. On average, they are thin relative to lumen area. Porosity is finely dispersed, and original texture and structure are well preserved. Occasional incipient structural collapse can be observed at the margin of fragments. Cases of complete replacement of fragments and mineralisation are evident from sharp shifts in reflectance. High reflectance inertinite is dominant, fusinite is prevalent, mineral matter content is low. BC2 can be placed predominantly in the

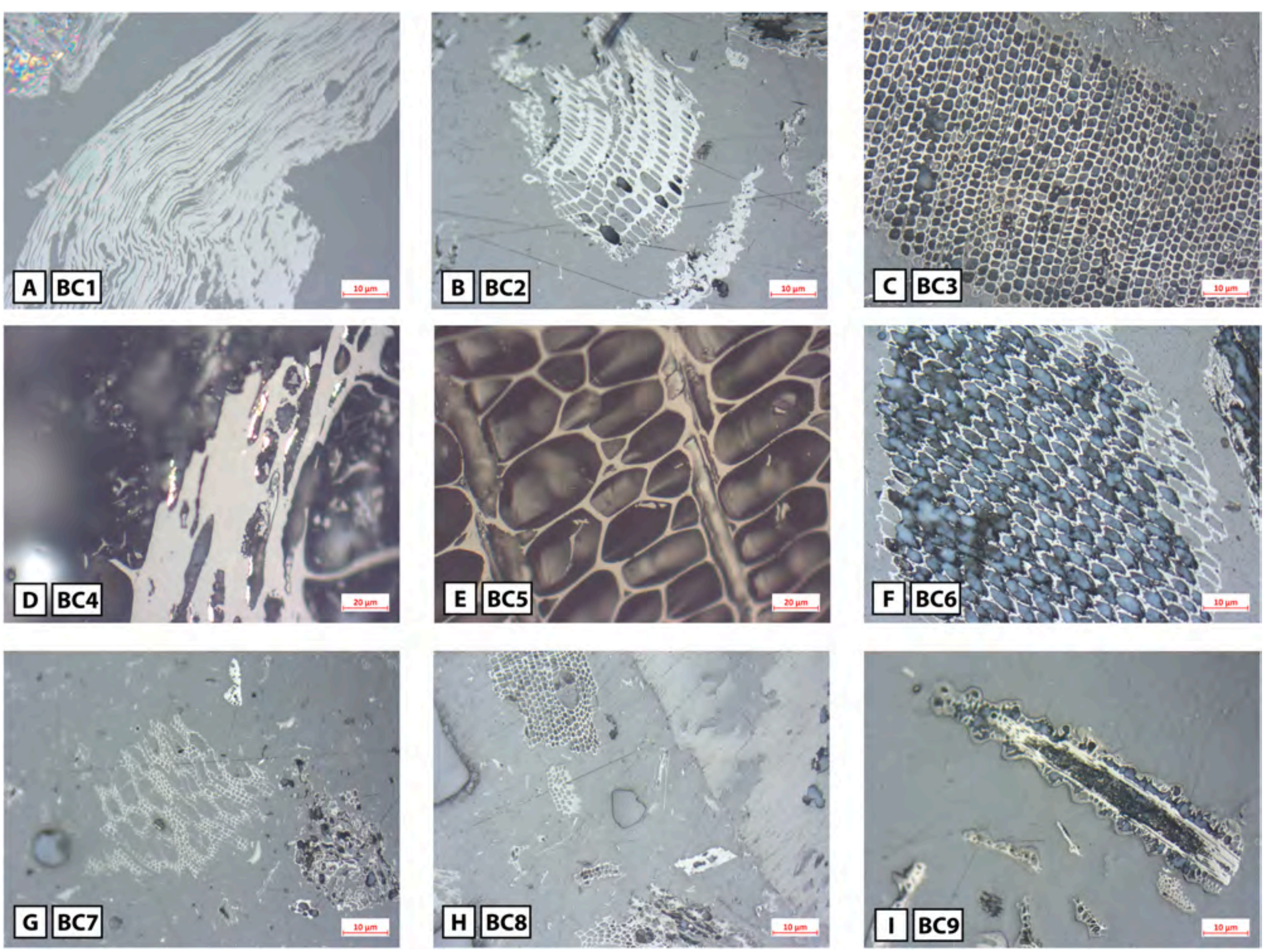

Fig. 3. Representative microphotographs of optical analysis under reflected monochromatic light of biochar samples. A) BC1; B) BC2; C) BC3; D) BC4; E) BC5; F) BC6; G) BC7; H) BC8; I) BC9. See text for detailed description.

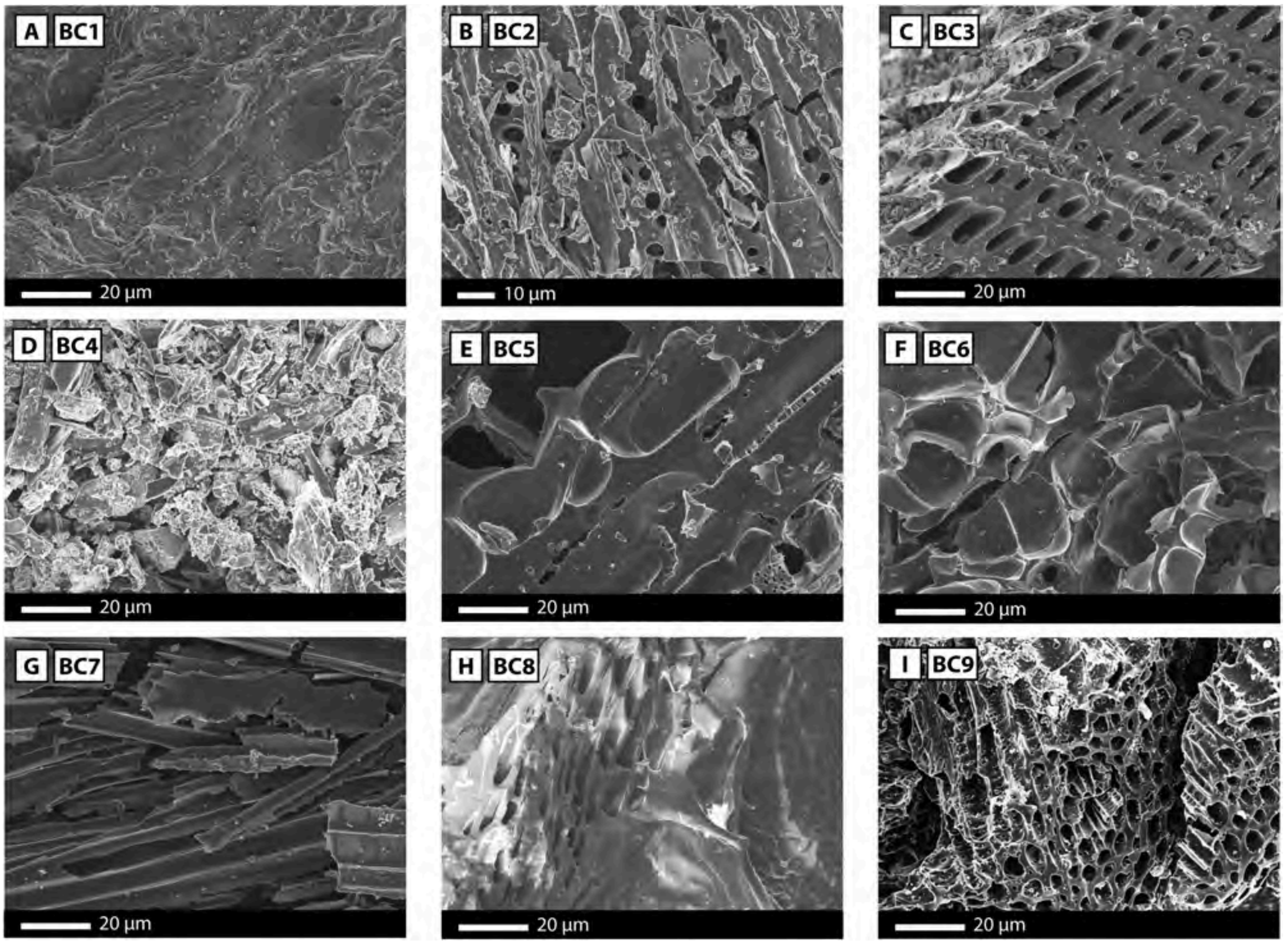

Fig. 4. Representative SEM images of biochar samples.) BC1; B) BC2; C) BC3; D) BC4; E) BC5; F) BC6; G) BC7; H) BC8; I) BC9. See text for detailed description.

inertoid category with >75 % unfused material. The sample fragments are mainly homogeneous. SEM images display fragment-scale fractures damaging otherwise well-preserved plant structures. Presence of additional, smaller fragments characterized by a rougher surface is detected.

BC3 (Figs. 3C and 4C) - Optical images of sample BC3 display very well preserved perpendicularly and obliquely cut cell walls and lumens with no alteration, even at margins. The original plant structure is preserved and homogeneous, characterised by rather large cell lumens and thin walls. The material is composed of elongated fragments with a bimodal size distribution. Larger fragments are less common and dispersed throughout the finer material. The sample is uniform in terms of white colour intensity. BC3 can be placed predominantly in the inertoid category with >75 % unfused material. SEM images display well preserved structures with no infilling.

BC4 (Figs. 3D and 4D) - Optical images of sample BC4 display perpendicularly cut, well preserved plant structures. Walls are comparatively thick with respect to lumens. No fractures, collapses or alterations can be observed. Signs of mineralization are present. High reflectance inertinite is dominant, fusinite is prevalent and mineral matter content is low. White level is uniform for all fragments in the sample. BC4 can be placed predominantly in the inertoid category with >75 % unfused material. SEM images essentially show two kinds of fragments. One is characterized by smooth surfaces and angular shape, the other by rough surfaces and globular shape. No visible porosity is to be found and no visible plant structures can be observed in collected images.

BC5 (Figs. 3E and 4E) - Optical images of sample BC5 show well-preserved plant structures. There is evidence of both thick and thin cell walls. Traces of structural collapse can be observed at fragment margins. Lumens and walls are more regular in areas characterized by thin walls in relation to cell lumens. In contrast, areas where walls are thicker appear more chaotic and affected by lumen collapse. High reflectance inertinite is dominant, fusinite is prevalent and mineral matter content is low. White level is uniform for all fragments in the sample. BC5 can be placed predominantly in the inertoid category with >75 % unfused material. SEM images of BC5 display well-preserved plant structures and clean smooth surfaces. Occasional, very fine, angular and globular fragments are present.

BC6 (Figs. 3F and 4F) - Optical images of sample BC6 show well-preserved plant structures with thin walls and large lumens. In areas where cell walls appear to be thicker, lumens are irregularly shaped indicating incipient structural collapse. There is no evidence of fracturing. Mineralisation is limited, but present. Finely cellular porous texture is detected. High reflectance inertinite is dominant, fusinite is prevalent. White level is uniform for all fragments in the sample. BC6 can be placed predominantly in the inertoid category with >75 % unfused material. SEM images of BC6 show large fragments of well-preserved material where structural organization is still clearly recognisable. Surfaces are smooth although a sparse groundmass of smaller smooth fragments is present.

BC7 (Figs. 3G and 4G) - Optical images of sample BC7 show different types of fragments indicating non-uniform feedstock. The first abundant category (around 80 %) is made up of structured fragments with pore-to-wall fragments either high or extremely low, with original tissue well preserved and almost homogeneous white colour. The second abundant category is made of fused biomass with the highest pore-to-wall ratio in the sample, wall colour bright white, and sub-rounded generally equi-dimensional fragments and pore borders. High overall thermal maturity is supposed. Partial filling by biochar fragments of smaller pores is observed. Pore-filling by opaque inorganic material (possible mineralisation) can be observed, as well. BC7 can be placed predominantly in the inertoid category with >75 % unfused material. SEM images show elongated fragments with clean smooth surfaces, alongside with little, sparse groundmass. A rougher surface is observable in correspondence of some fragments, but elongate shape and overall structure are still well recognisable.

BC8 (Figs. 3H and 4H) - Optical images of sample BC8 display fragments characterized by thin walls and areas of irregular porosity. Such fragments have a high grade of homogenization. In other fragments the original structural organization appears to be intact, and walls are thin. These observations suggest the likely presence of multiple feedstocks reacting differently to heating. Porosity is clean with no fillings. Traces of fracturing can be observed at the margins of some fragments. No mineralization is detected. White level varies, but thermal maturity is generally high. High reflectance inertinite is dominant, fusinite is prevalent. White level is uniform throughout the fragments in the sample. BC8 can be placed predominantly in the inertoid category with >75 % unfused material. SEM images show well preserved plant structures characterized by smooth surfaces. Some globular shaped infilling is present in correspondence of specific lumens, but porosity remains open overall.

BC9 (Figs. 3I and 4I) - Optical images of sample BC9 show well-preserved plant structures. Obliquely and perpendicularly cut cell lumens are bounded by thin cell walls. Fragments are generally elongated and show signs of incipient alteration along margins. Smaller fragments with the same characteristics are present as well. No mineralization can be observed. The sample is uniform in terms of fragment size and white colour intensity. BC9 can be placed predominantly in the inertoid category with >75 % unfused material. SEM images display large fragments of well-preserved plant structures alongside with smaller fragments where only remnants of such structures are still detectable. The smooth surfaces of plant structures are covered by a sparse, very fine groundmass of globular shaped foreign matter.

3.1.1. *Energy dispersive x-ray spectroscopy (EDX)*

EDX results highlight that all biochar bear between 80 % and 92 % carbon atomic content, except for BC9 where carbon is 78 % (Fig. 5). The second most abundant component is oxygen (between 6 % and 18 %, atomic). Depending on the biochar other elements occur, as well in traces (Fig. 5). Potassium is present in all but BC8; calcium occurs in all biochar except BC8 and BC9. Silicon EDX results highlight that all biochar bear between 80 % and 92 % carbon atomic content, except for BC9 where carbon is 78 % (Fig. 5). The second most abundant component is oxygen (between 6 % and 18 %, atomic). Depending on the biochar other elements occur, as well in traces (Fig. 5). Potassium is present in all but BC8; calcium occurs in all biochar except BC8 and BC9. Silicon has been detected in both BC2 and, in a much greater concentration, in BC9. Small amounts of magnesium have been observed in BC6 and BC7. Phosphorus has only been found in BC6. These results are generally in agreement with ranges indicated in literature (Weber and Quicker, 2018). Moreover, despite the whole composition being related to the feedstock's nature, carbon and oxygen content (alongside with hydrogen) are mostly affected by pyrolysis conditions. Minor components tend to rise from the feedstock's specific chemical makeup.

3.1.2. *X-ray diffraction (XRD)*

The XRD analysis yields an assemblage dominated by amorphous matter that range from 64 % (BC7) to 100 % (BC1), with six samples out of nine (BC1, BC2, BC4, BC6, BC8, BC9) containing >90 %. Quartz is ubiquitous and occurs as a minor phase, either in traces or with low content ranging between 1 % and 5 %. Calcite is ubiquitous as well, showing values lower than 8 %, apart in samples BC3 and BC7 that contain 13 % and 23 %, respectively. Other phases such as Plagioclase, Phyrrotine traces are detected only in sample BC4, as well as Sylvite in sample BC9.

3.1.3. *Ion coupled plasma mass spectroscopy (ICP-MS)*

The objective of ICP-MS analysis was to determine the nature and concentration of trace substances present in commercial biochar. Fig. 7 shows results of ICP-MS analysis of the nine biochar divided among arbitrary categories depending on their concentration.

In Fig. 7A, major metal content ranges from close to 10.0 % down to 0.02 %. Most of them show concentrations that are comprised between about 0.1 % and 1.0 % with the exceptions of BC7 that bears the highest concentrations, and the BC1 that rarely exceeds 0.1 %. On average, Calcium is the most abundant element and Sodium is the least abundant.

In Fig. 7B, heavy metal content is highly variable, ranging from >150.0 ppm down to 0.2 ppm. On average, the most abundant heavy metal is Zn. All elements but As and Cd are present in all nine biochar. As is absent in BC1, Cd is absent in BC1, BC2, BC3, BC6 and BC8. Cd is also the least abundant heavy metal when present. BC7 bears the greatest heavy metal content, while BC1 bears the lowest overall.

In Fig. 7C, other elements present in all nine biochar in the order of tens to hundreds of ppms are Mn, Rb, Ba and Sr. Among them, Mn is the most abundant and Rb the least abundant. On average, highest contents are recorded in BC7, although BC9 has much higher Mn concentration (749 ppm in BC9 vs. 435 ppm in BC7).

In Fig. 7D, other trace elements present in all nine biochar are Cs, Co, Mo, La, Ce, Nd. Their concentrations range from 0.06 up to about 7.00 ppms. On average, greatest contents are recorded by BC7 and lowest ones by BC1.

In Fig. 7E, elements in this category are present in more than half of

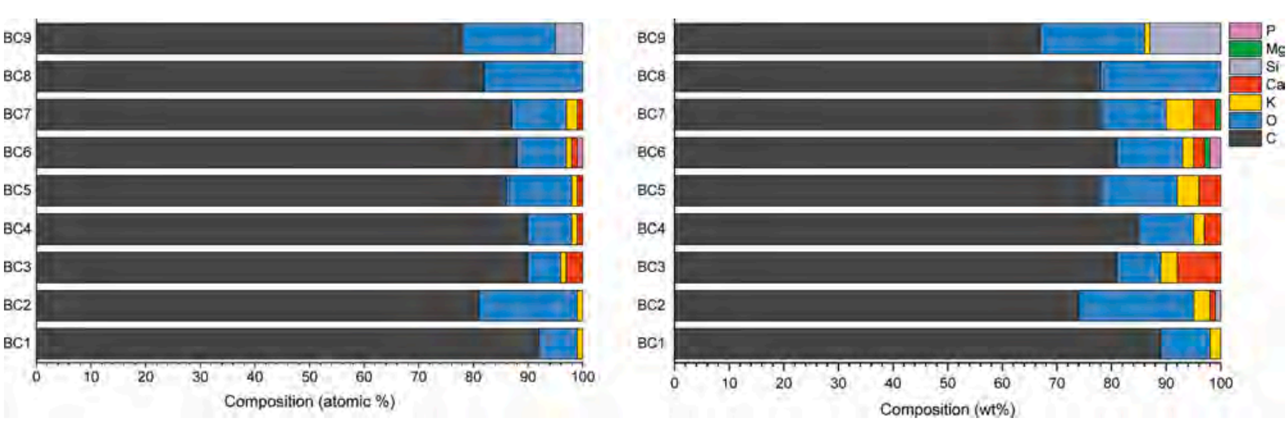

Fig. 5. EDX data on biochar samples. Left: Percentage atomic composition (values are approximate to zero for element in trace); right: Percentage weight composition. See supplementary materials for numerical data and descriptive statistics.

the biochar. Concentrations range from 0.04 up to few ppms, but rarely exceed 1 ppm. If present, elements are usually more abundant in BC7. Concentrations in other biochar samples are highly variable.

In Fig. 7F elements are present in less than half of the biochar. Concentrations are below 1 ppm. The only biochar containing all of these elements is BC7. Some of these elements are also present in BC3 and BC5, but absent in the remaining biochar.

3.1.4. PH and electric conductivity (EC)

PH is basic for all biochar samples ranging from a minimum of 8.0 in BC8 and a maximum of 12.42 in BC7 (Fig. 8). Six out of the nine biochar sit between pH 9.5 and 10.5 forming a cluster (BC1, BC2, BC3, BC5, BC6, BC9). Electric conductivity (EC) ranges from 230 μS in BC1 up to 2417 μS in BC7. Electric conductivity grows exponentially with pH.

3.1.5. Fourier transform infrared spectroscopy (FT-IR)

The FT-IR spectra were used to provide the main functional groups based on the main spectral regions (Fig. 9): ν_{O-H} (-OH group, 3600–3200 cm^{-1}), aromatic ν_{C-H} region (3100–3000 cm^{-1}), aliphatic ν_{C-H} region (3000–2800 cm^{-1}), $\nu_{C=O}$ (saturated and/or aromatic carbonyl groups $C = O$), and $\nu_{C=C}$ stretching bond of unsaturated aromatic and/or alkene groups (1710–1550 cm^{-1}), asymmetric aliphatic CH_2 and CH_3 and/or aromatic skeletal vibrations combined with C–H in-plane deformations (complex peaks around 1,440 cm^{-1}), aliphatic symmetric CH_3 deformation (peak around 1375 cm^{-1}), aromatic and/or aliphatic ether and alcohol ν_{C-O} vibrations (1300 and 900 cm^{-1}), and aromatic out-of-plane C—H deformation region (900–650 cm^{-1}).

In all samples, a broad absorption band (3200–3600 cm^{-1}) corresponding to the ν_{OH} group is present. After oven treatment, collected spectra decreased in the intensity of absorbance in this region. In the majority of biochar samples, the aromatic 3100–3000 cm^{-1} (e.g., BC2, BC5, BC6, BC8, BC9) and the aliphatic 3000–2800 cm^{-1} (BC1, BC2, BC4, BC5, BC6, BC8, BC9) C—H stretching regions are present and characterized by weak relative absorbance intensities, except in BC3 and BC7, where the aromatic and aliphatic signals resulted totally absent (see Table 3).

For BC2, BC4, BC5, BC6, BC8, BC9 samples, the oxygenated group and aromatic carbon region 1710–1550 cm^{-1}, as defined in Mastalerz et al. (2023), display mainly four characteristic peaks in correspondence of the 1700, 1660, 1630 and 1565 cm^{-1} positions, whereas they are notably reduced or absent in BC1, BC3 and BC7. In this range, between 1710–1660 and 1630–1565 cm^{-1}, associated to the stretching modes of the oxygenated (ν C═O) and aromatic (ν C═C) groups respectively (Adhikari et al., 2024; Reza et al., 2020; Phan et al., 2021). BC2, BC4, BC5 and BC8 show peaks associated to aromatic compounds around 1640–1,550 cm^{-1} for ν C═C and lower intensities at 1710–1640 cm^{-1} for saturated and/or aromatic carbonyl groups, such as carboxylic acids, ketones and esters (ν C═O). In detail, BC4 lacks in ν C═O vibration of carbonyl group at 1700 cm^{-1}, while in BC2 and BC8, the aromatic C═C stretching vibration is shifted to 1585 cm^{-1} respect to BC4 at 1565 cm^{-1}. In the same regions (e.g., 1710–1660 and 1630–1565 cm^{-1}), BC5, BC6, and BC9 exhibit fewer peaks and relatively lower absorbance intensities of oxygenated stretching around 1565 and 1690 cm^{-1} respect to aromatic ν C═C bounds.

All FT-IR spectra exhibited bands around 1454–1430 cm^{-1}, which are typically attributed to the asymmetric d of -CH_2 and -CH_3 aliphatic hydrocarbons in coal and kerogen (Caricchi et al., 2016; Chen et al., 2012; Di Paolo et al., 2012; Lis et al., 2005). However, in the case of biochar, this range is more likely associated with unsaturated aromatic C═C skeletal vibrations combined with C—H in-plane deformations, originating from lignin derived products after pyrolysis (Keiluweit et al., 2010; Md Salim et al., 2021). Furthermore, in BC1, BC2 and BC8, signals between 1375–1385 cm^{-1} are present, probably associated to overlapping vibrations from the symmetric deformation of aliphatic -CH_3 groups and/or in-plane absorption of phenolic -OH groups. These signals are related to cellulose and lignin feedstocks (Ilić et al., 2022; Keiluweit et al., 2010), with low intensities detected in samples BC5, BC6, and BC9.

The broad band between 1300 and 900 cm^{-1} (with maximum around 1032–1088 cm^{-1}, e.g., BC1, BC4, and BC9) may contain overlapping

Table 3
Assignment of the main functional groups (in green, when present).

ADSORPTION BAND REGIONS AND FUNCTIONAL GROUPS [cm^{-1}]	BIOCHAR BAND ASSIGNMENT								
	BC1	BC2	BC3	BC4	BC5	BC6	BC7	BC8	BC9
3600-3200 -OH stretching in hydroxyl group	●	●	●	●	●	●	●	●	●
3100-3000 Aromatic C-H stretching		●			●	●		●	●
3000-2800 Aliphatic C-H stretching	●	●		●	●	●		●	●
1710-1690 C=O stretching of carbonyl groups		●	●		●			●	
1690-1640 C=O stretching conjugated with aromatic rings		●	●		●			●	
1640-1550 C=C stretching in aromatic rings and/or alkane group		●		●	●	●		●	●
1454-1430 Asymmetric aliphatic CH_2 and CH_3 deformation or C-C stretching	●	●	●	●	●	●	●	●	●
1385-1365 Symmetric aliphatic CH_3 deformation	●	●						●	
1250-1030 C-O and/or O-H stretching in methoxy group	●	●	●	●	●	●	●	●	●
880-750 Aromatic out-of-plane C-H deformation bands		●			●	●		●	●

peaks which can be assigned to aromatic -OH and CO- and/or aliphatic ether and alcohol ν C—O. These are probably associated to undecomposed cellulose and hemicellulose material (Ilić et al., 2022; Keiluweit et al., 2010; Reza et al., 2020). In detail, in BC1, BC2, BC4, BC8, and BC9, these signals are well evidenced. In the lowest analysed range interval, BC2, BC5, BC6, BC8, and BC9 show the aromatic out-of-plane C—H deformation bands between 900 and 700 cm^{-1} (Caricchi et al., 2016; Mastalerz et al., 2023) characterized by rather irregular few peaks with relatively low absorbance intensities.

3.2. Sampling survey

Surface waters from the four sampling points in the Malagrotta landfill area were analysed to determine pollutant concentrations (Fig. 10). The results, together with the associated detection limits are summarised in Fig. 10 and related to chemical drinking water thresholds according to Italian legislation (D.Lgs., 2023). The drinking water regulation is employed to provide a meaningful water quality standard for comparison.

Fig. 10 displays concentrations for Mg, Na, sulphates and chlorides; they are within drinking water limits at all sampling points. They also display the same behaviour in terms of abundance. The concentration increases going downstream and is greater in the tributary stream with respect to the main river. This is a consequence of dilution. Fluorides and nitrates behave differently being more abundant in correspondence of the MU sampling point when compared to MD. On the other hand, their content still increases going downstream through the tributary. Nitrites have only been detected in correspondence of the MD sampling point in minimal amounts (Fig. 10).

In terms of trace chemicals (Fig. 10) Sb, Cd, Hg, Pb, Cu, Se and cyanides could not be detected. Cr is only present at TD with a concentration of 1 μg/L (Fig. 10) . Ni has only been detected in sampling points of the tributary stream (Fig. 10). It increases from 8 to 11 μg/L going downstream between the two (Fig. 10). based upon above concentrations presence of Ni sources along the tributary stream could by hypothesized. Such Ni content is then likely to be diluted below detection limit upon entering Rio Galeria. V is present at sampling sites at concentrations between 5 and 15 μg/L (Fig. 10). Such concentrations are greater throughout the main watercourse but still below the drinking water limit. As found at all the sampling points in an abundance rising going downstream in the hydrographic network. The threshold for As in potable water, 10 μg/L, is breached in three out of the four sampling points with a maximum concentration of 19.4 in correspondence of MD. These are the only exceedances in the dataset. However, As content is tied to a higher natural background rather than anthropogenic activity due to the study area rising above As rich volcanic deposits (Barbieri et al., 2014).

3.3. Effects of environmental waters on biochar surface structure

The experiment was aimed at monitoring changes in biochar as a consequence of river water treatment. Due to low contaminant concentrations in river water when compared to contents already present in biochar no significant evaluation could be performed in this regard. In fact, changes in terms of biochar composition could both be attributed to interaction with river water and natural variability of the material itself (Figs. 7, 10). Nevertheless, biochar employed for water treatment has been observed through scanning electron microscopy to survey changes occurring on biochar surface. Three main categories of alterations could be observed: surface degradation, pore filling and foreign matter adsorption. Prominent examples of the end members of these processes are shown in Fig. 11. In Fig. 11 (A-A') continuous surfaces display degradation after the adsorption process. Cavities are developed disrupting continuity and smoothness of the original surface. In Fig. 11 (B-B') porosities present in pristine material become occluded by foreign fragments. In Fig. 11 (C-C') smaller scale foreign fragmental material appears on previously clean surfaces.

3.4. Leaching of contaminants into mineral water

A leaching test has been conducted to verify that biochar does not cause significant harm to water quality. Effect of biochar exposure has been tested against store bought mineral water for 24 h using a dosage of 10 g/L. Such a dosage constitutes a common upper limit of adsorption experiments as testified by (Dinh et al., 2022; Mahdi et al., 2018; Mohan et al., 2007). Fig. 12 displays leaching happening but being limited to values not breaching drinking water thresholds. This is true for both major contaminants and trace elements.

4. Discussion

Comparing biochar FT-IR spectra in relation to their feedstocks of plant origin (Table 1), we observe no significant differences among them. All spectra show peaks between 1600–1400 cm^{-1} (e.g., with shared peak around 1442 cm^{-1}) typically derived from lignin, cellulose, and hemicellulose products particularly evident in BC2, BC4, BC5, BC6, and BC8 (Adhikari et al., 2024; Keiluweit et al., 2010; Mastalerz et al., 2023). After oven treatment, collected spectra decreased in the intensity of absorbance in the hydroxyl -OH region (3600–3200 cm^{-1}). This feature is likely due to the O—H stretching in "free" water molecules (non-hydrogen-bonded) and/or coincident with the stretching vibrations in alcohols, carboxylic, and phenol groups (Ilić et al., 2022; Keiluweit et al., 2010). It is excluded that -OH group is part of sorbed water in hydrous expandable clay minerals (Singh et al., 2016).

All biochar samples share a general feature in the oxygenated group and aromatic carbon region 1710–1550 cm^{-1}: low intensity in oxygenated functional groups, around 1700 cm^{-1} in particular (C═O stretching), coupled with high intensity between 1690–1640 cm^{-1} and 1640–1550 cm^{-1}, associated to conjugated aromatic stretching of C═O and C═C bonds, indicating a high degree of aromatic structure condensation. Oxygenated functional groups, such as hydroxyl, carboxyl and carbonyl, show low intensity or absence as production temperatures increase. For example, in BC3 and BC7, produced through pyro-gasification up to 850 C°, oxygenated functional groups have low intensity (Fig. 9). On the contrary, in BC5, with pyrolysis up to 550 °C, they are well distinguishable. FT-IR spectra of BC1 and BC9 suggest lower pyrolysis maximum temperatures compared to the other studied biochar. Broad and intense peaks observed at 1032 cm^{-1} for BC1 and 1088 cm^{-1} for BC9 are associated with the presence of undecomposed cellulose and/or lignin fraction (Ilić et al., 2022; Keiluweit et al., 2010; Reza et al., 2020).

Photographs of biochar samples (Fig. 1) and macroscopic description in Table 1 display significant variability in fragment shape and size, depending on both feedstock and production process. The relative importance of these two factors is ruled by biochar type. For example, in BC1 the process of palettization alters the original shape of the fragments. Conversely, particle size and morphology remain unchanged during production process as reflecting the rice husk feedstock of BC9. Macroscopically, the different biochar types sit between these two end-members. Most materials are provided with a heterogeneous grain size; only three out of the nine biochar are homogeneous (BC1, BC2, BC9). Some manufacturers do also offer biochar with specific granulometric distributions. Presence of ashes is a common occurrence as well. The only materials where their presence is negligible are BC2, BC4 and BC9. Two biochar come humid out of the box (BC4 and BC9), while the others are essentially dry.

Overall, the optical properties of biochar samples are similar. They are characterized by dominance of high reflectance inertinite and prevalence of fusinite. All biochar samples belong to the inertoid category (>75 % unfused material and up to 40 % porosity) according to the classification proposed for the first time by Lester et al. (2010) and modified by Mastalerz et al. (2023). Differences are related to fragment shape, mineralisation, fracturing degree, alteration and pore area-to-wall thickness ratio. They relate to both feedstock and production process (Hassan et al., 2020; Ippolito et al., 2020; Rajput et al., 2024; Tomczyk et al., 2020; Yargicoglu et al., 2015). In detail, mineralisation is favoured by availability of suitable molecules (e.g., carbonates) and high production temperatures (Lian et al., 2021; Zhao et al., 2015; Zheng et al., 2013). Fracturing and alteration can be the result only of thermal degradation, whereas feedstock certainly constitutes the main controlling factor on pore area-to-wall thickness ratio, keeping production temperature and heating rate constant (Mastalerz et al., 2023; Werdin et al., 2020).

Traces of mineralisation detected under the microscope relate to samples BC3, BC4, BC6 and BC7 (Fig. 3), are also confirmed by XRD analyses (e.g., mainly calcite) (Fig. 6). The optical survey also indicates occurrence of thermal alteration in samples BC8 and BC9. In the former, alteration appears to be confined to one portion of the feedstock highlighting its initial heterogeneity. In the latter, alteration is limited to fragment margins indicating incipient thermal alteration processes and thus unable to cause full changes in the material (Morga, 2010, 2011).

Composition of analysed biochar falls within literature ranges for lignocellulosic feedstocks. Carbon represents the greatest part of the material (Hassan et al., 2020; Huang et al., 2019; Weber and Quicker, 2018). EDX results are broadly consistent with XRD where carbon and oxygen are predominant and make up the amorphous carbonaceous fraction of the material (Clemente et al., 2018; Hou et al., 2016; Keiluweit et al., 2010; Oleszczuk et al., 2016). However, it is worth noting that a higher amount of carbon and oxygen does not necessarily correspond to a higher amount of the amorphous organic fraction, as C is also fixed in calcite (Clemente et al., 2018; Hou et al., 2016). Prominent examples are samples BC3 and BC7 with 90 % and 87 % carbon content (Fig. 5), are among the richest in carbon in the dataset. Despite this fact, the amorphous fractions of such carbons (Fig. 6) are the lowest in the dataset due to presence of significant amounts of calcite (13 % in BC3 and 33 % in BC7).

The ICP-MS results were mainly used to determine trace contaminant contents already present in the biochar, with a focus on heavy metals. Fig. 7 testifies that heavy metals are essentially present in all biochar samples, at least to some extent. Their concentration range from below 1 to over 100 ppm. Zinc and cadmium are the most and least abundant elements, respectively.

The study area is the hydrographic network surrounding the decommissioned Malagrotta landfill. It was identified with the support of local environmental authority. The choice was based on the area's long and controversial history, as well as water quality indicators available in public reports (SIRA, 2024). These reports provide general and qualitative descriptions indicating bad water conditions but do not include analytical data, highlighting the need for further investigation.

A new sampling survey was performed (Fig. 2). Analytical results revealed that chemical composition of surface waters were not alarming. On the contrary, they were below the limits for drinking water established by the Italian government (D. Lgs., 2023).

Survey results for major chemicals (Fig. 10) show higher concentrations at TU and TD sampling points along the tributary stream. Such amounts increase moving downstream. They are also greater with respect to MU and MD points along the main river. Concentrations at TU and TD are likely due to the limited amount of water present in the tributary stream compared to the main river. Along the main river substances are much more affected by dilution (MU and MD). For detected trace contaminants (Fig. 10), overall concentrations in the tributary stream are lower than those recorded along the main river. This means that the input coming from sources along the tributary is negligible compared to those along the main river. This phenomenon is exemplified by Nichel's behaviour throughout the four sampling points. Nichel is absent in MU and MD but is present in TU and TD, increasing as one goes downstream. This fact implies a source along the tributary ad subsequent dilution after confluence into the main river. Sampled water has also been employed to check possible changes of biochar surface structure due to interaction with environmental waters, as suggested by literature (Das and Sarmah, 2015; Goñi-Urtiaga et al., 2022; Spokas et al., 2014).

The contaminant concentration ratio between surface water and biochar is a fundamental parameter to consider while evaluating adsorption processes. In this study feasibility of biochar treatment for surface water bearing very low contaminant concentration is explored through high resolution techniques in ICP-OES and ICP-MS. A comparison of the obtained results evidenced that trace elements are more abundant in biochar samples than in water. This does not allow detection of adsorption on biochar.

Another potential issue associated with biochar usage is leakage of contaminants from the biochar itself. This is especially true if significant concentrations are already present in the original feedstock (Kim et al., 2020). Biochar employed in this study contains considerable concentrations of heavy metals and other trace contaminants (Fig. 7). Leaching tests have been performed to assess safety for a potential environmental

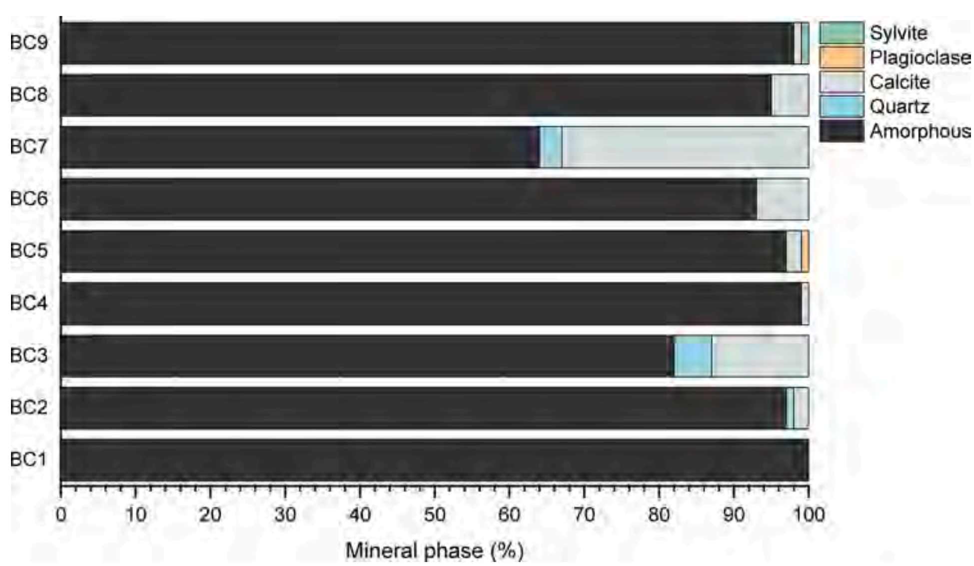

Fig. 6. Semiquantitative XRD composition of biochar samples, expressed in percentage. Note the prevalence of amorphous matter throughout all biochar samples. See supplementary materials for numerical data and descriptive statistics.

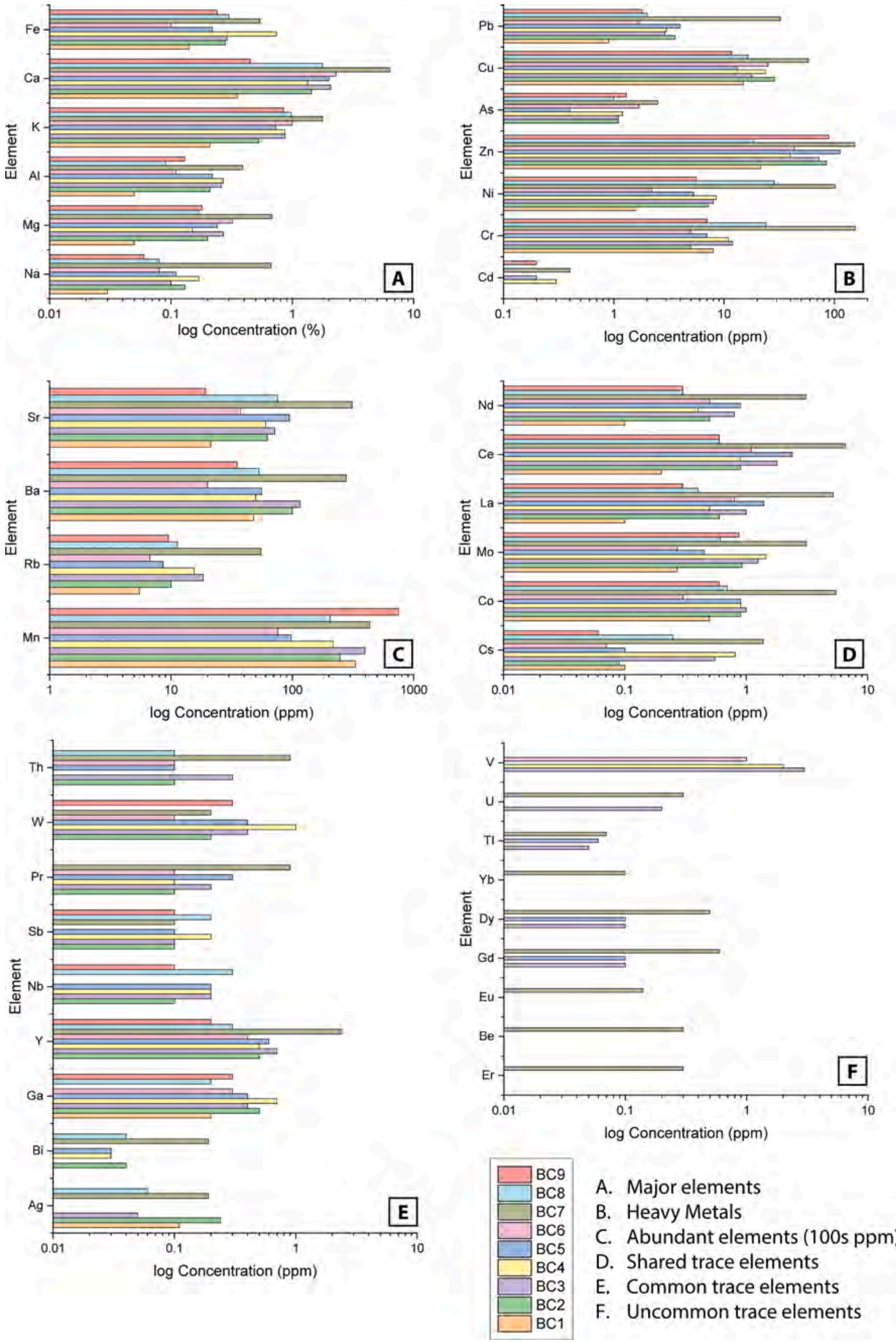

Fig. 7. Quantitative ICP-MS data on biochar samples, showing element concentrations (% or ppm, logarithmic scale). See supplementary materials for descriptive statistics.

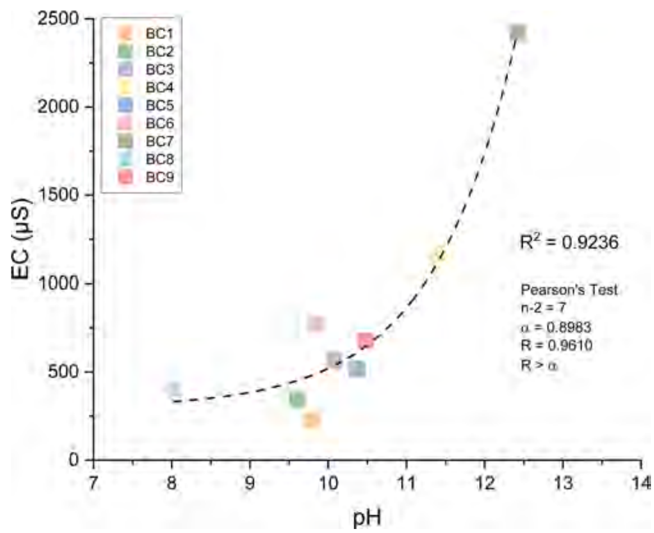

Fig. 8. PH and electric conductivity (EC) values of biochar samples. Reported values are averages of triplicate measurements, according to Singh et al. (2017). Pearson's test has been performed to ensure statistical soundness of the correlation.

application. Biochar dose (10 g/L) for leaching experiments was chosen according to upper optimal dosages used in synthetic adsorption experiments of heavy metals (Mohan et al., 2007; Li et al., 2013; Chen et al., 2022; Zhang et al., 2023a; Bayar et al., 2024). The matrix (mineral water) represents a bottom threshold for biochar use in terms of contamination. Testing leaching in this way guarantees safety also in less critical conditions, characterized by lower dosages and higher dissolved contaminant concentrations (Sun et al., 2022; Zhang et al., 2023b; Iamsaard et al., 2022; Van Hien et al., 2020). Moreover, in such instances, the impact of leaching is comparatively less crucial with respect to the removal potential.

The results confirm some leaching from biochar. However, this is limited to few ppms (Fig. 12) and does not compromise water quality to an extent that would make it unsuitable for its intended use. This is especially important considering employed dosages in this study, which are at the upper end of those commonly applied in adsorption experiments (Dinh et al., 2022; Li et al., 2013; Mahdi et al., 2018; Mohan et al., 2007; Moyo et al., 2016).

5. Conclusion

5.1. Research outcomes

Nine commercial biochar from Italy, France and Germany, produced by either pyrolysis or pyro-gasification, have been characterized to

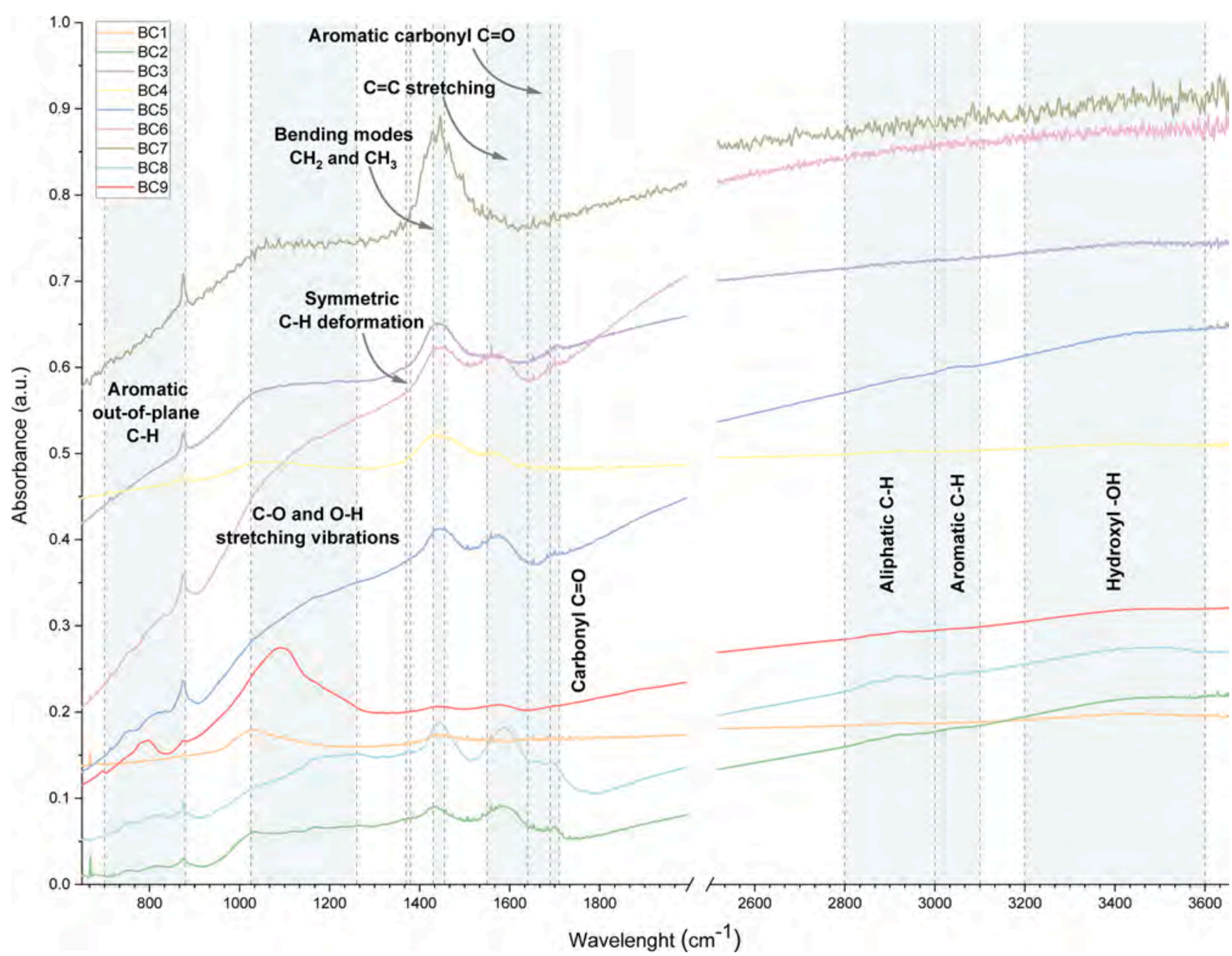

Fig. 9. Comparison among representative normalized FT-IR spectra for biochar samples. The band areas, representing the main functional groups, are highlighted in light grey. Due to variations in absorbance intensities, characteristics of each biochar are not always clearly distinguishable in the figure. For detailed observations, single spectra are provided in the supplementary materials.

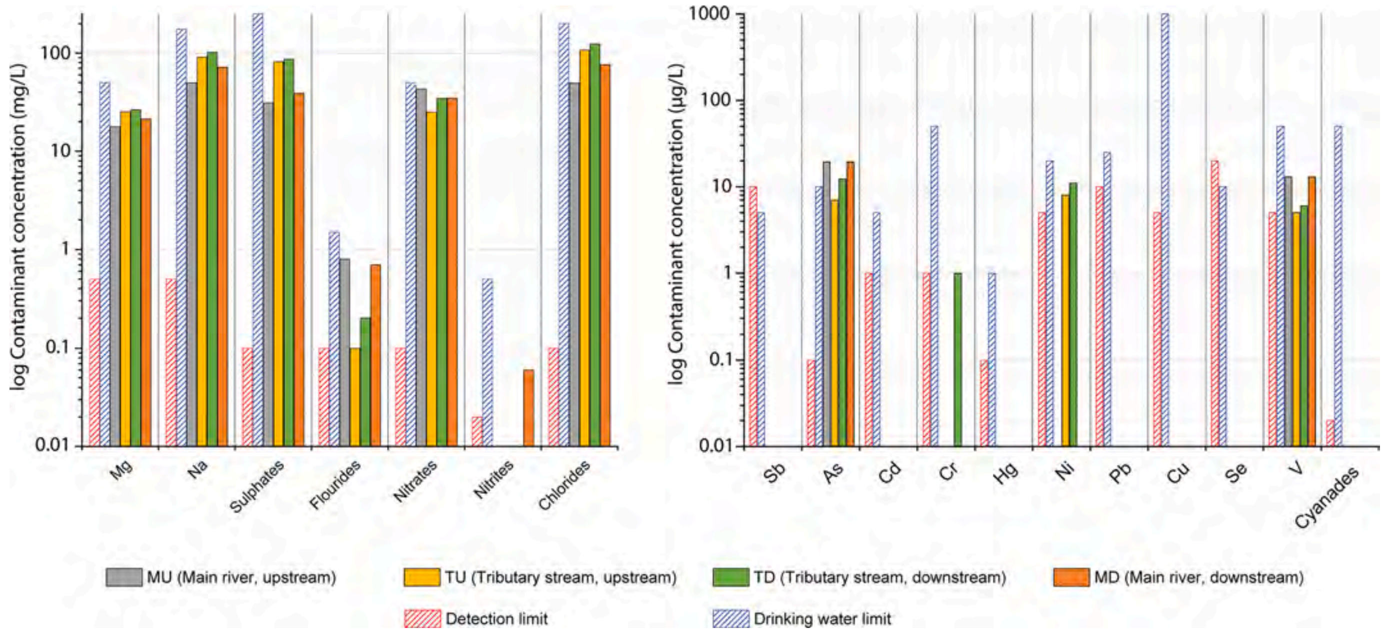

Fig. 10. Contaminant levels for the four sampling points, alongside detection limits and drinking water limits (logarithmic scale). Left: major contaminants in mg/L; right: trace contaminants in µg/L.

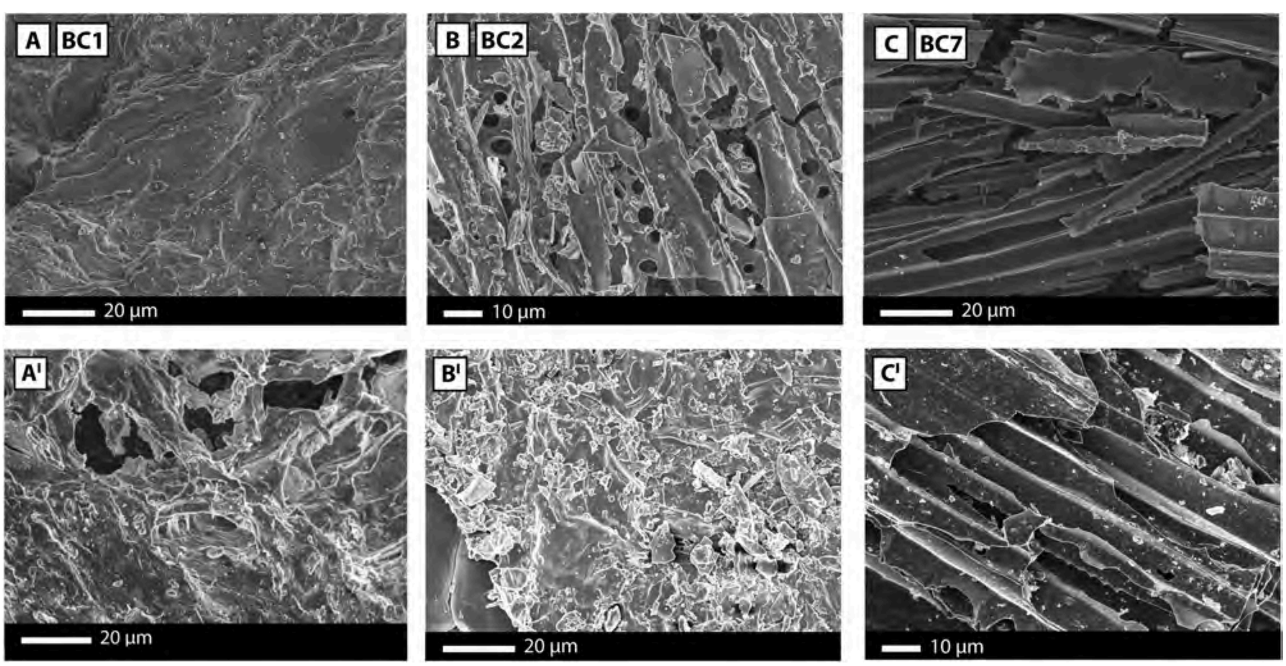

Fig. 11. Representative SEM images of the main observed types of biochar-environmental waters interaction; Left images (A, B, C): biochar before water treatment; Right images (A', B', C') post-treatment biochar. A-A') Surface degradation in sample BC1; B-B') Pore filling in sample BC2; C-C') Adsorption of foreign matter in sample BC7.

detect their physical-chemical properties. These biochar were tested with surface and mineral water todefine their physical-chemical modifications. The aim is to frame a potential biochar applicaton for environmental remediation through the case study of Malagrotta landfill.

Biochar properties are influenced by both feedstock and production processes (Janu et al., 2021; Tomczyk et al., 2020; Weber and Quicker, 2018; Zheng et al., 2013). Macroscopically common features are heterogeneous grain size and presence of ash. Shared optical property is the dominance of high reflectance inertinite. All samples fall within the inertoid class based on current coal char classification. Feedstock and production processes influence variations in fragment shape, mineralization, fracturing, alteration, and pore area-to-wall thickness ratio (according to Mastalerz et al., 2023). Mineralization is enhanced by suitable inorganic components, while fracturing and alteration result from physical stress (Zhao et al., 2021, 2015). These features are all enhanced by thermal degradation.

Bulk compositional analyses (EDX, XRD) testify coherence of commercial biochar with its laboratory counterparts underscoring carbonaceous content. The same goes for extensive properties: pH is basic for all biochar ranging from a minimum of 8.0 in BC8 and a maximum of

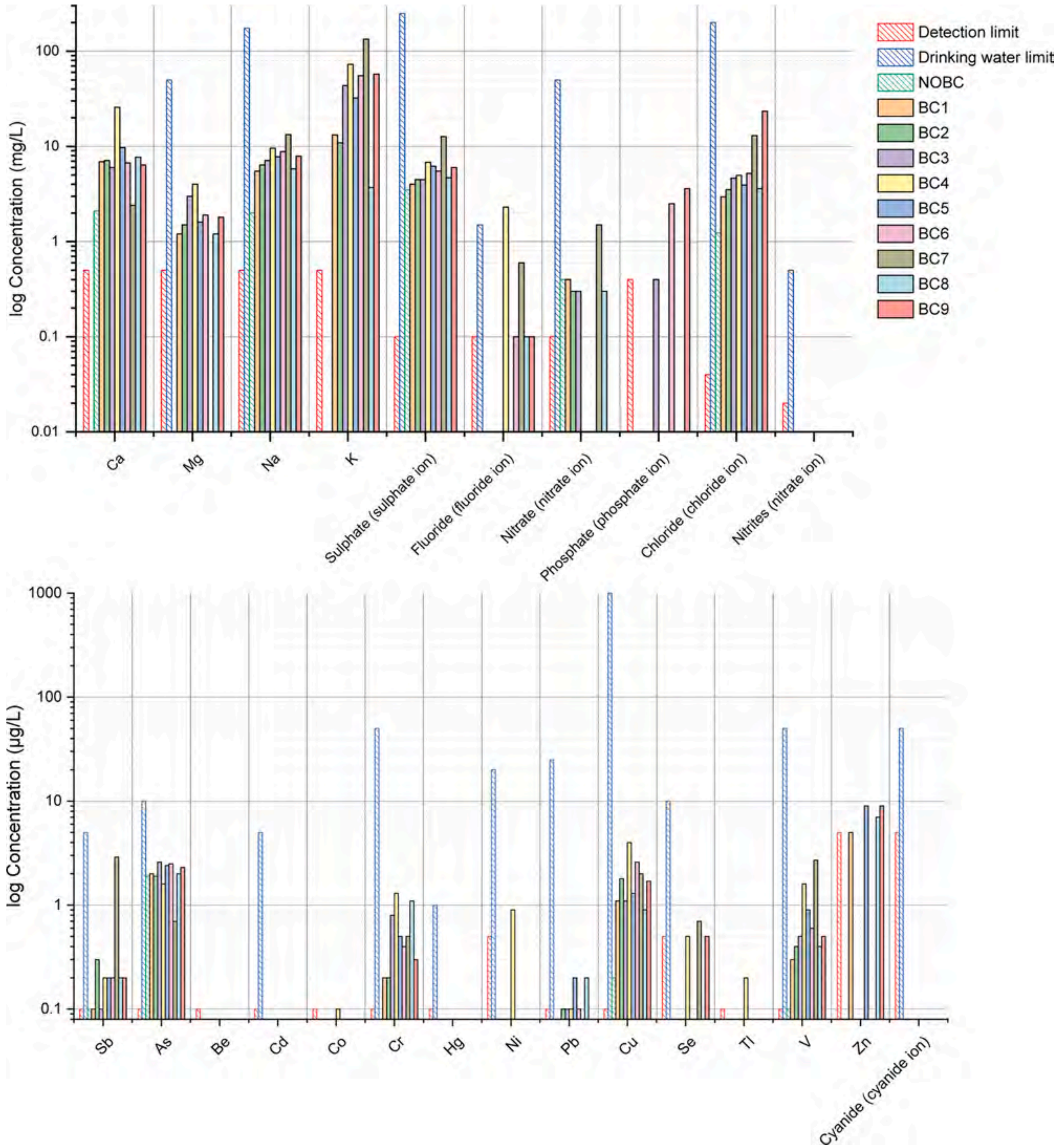

Fig. 12. Contaminant levels in water samples before (NOBC) and after the leaching testing (logarithmic scale). NOBC values relate to pristine mineral water. BC1 through BC9 relate to leaching of each biochar sample. Detection and drinking water limits are reported to aid interpretation. Top: major contaminants in mg/L; bottom: trace contaminants in μg/L. See supplementary materials for descriptive statistics.

12.4 in BC7. Electric conductivity (EC) ranges from 230 μS in BC1 up to 2417 μS in BC7. Electric conductivity grows exponentially with pH. ICP-MS (Fig. 7) was employed to survey trace element concentrations and compare them with those of surface water.

Surface waters belong to the decommissioned Malagrotta landfill area. Despite publicly available data testifiying scarce water quality levels, chemical contaminants mostly reside below drinking water thresholds. As a consquence, monitoring of adsorption perfomance on biochar is intrinsecally hindered. Biochar contaminant levels shadow changes in trace contaminant concentrations. Nevertheless, biochar-water interaction caused physical alteration on biochar (Das and Sarmah, 2015; Goñi-Urtiaga et al., 2022; Sorrenti et al., 2016). Observed phenomena were categorized in surface degradation, pore filling and adsorption of foreign matter. Leaching tests with 10 g/L dosage and mineral water were conducted in order to evaluate contaminant release from biochar and ensure safety. Leaching was detected but limited to few ppms, hence not significantly impacting original water quality.

Characterization of commercial biochar is necessary to select appropriate applications. Choosing a suitable context is equally important. The surface waters of the Malagrotta area did not bear high enough pollutant concentrations for biochar action to be properly detectable. Such a background is instrumental in establishing a bottom threshold for biochar application becoming especially important when it comes to trace element removal. Nevertheless, biochar would be safe to use even where adsorption results would not be satisfactory.

5.2. Future perspectives

These data can be employed to bring forth biochar specific water treatment policies, in particular regarding standardization. Such measures have already been put in place for activated carbon for treatment of water intended for human consumption in EN 12,903:2009, EN 12,915–1:2009 and EN12915–2:2009 (CEN, 2009a; 2009b; 2009c) Similar procedures could be developed for biochar for surface water treatment creating an analogous tool to standard EN 12,902:2004 concerning products used for treatment of water intended for human consumption (CEN, 2004). Additionally, guidelines for the characterization of the application context should also be included to ensure adherence to the European water framework directive 2000/60/EC (EU, 2000).

Biochar bears enormous potential for water purification. Further research efforts should concentrate in finding the best case scenarios for biochar application to exploit this potential to its full extent (Castiglioni et al., 2022; Dinh et al., 2022; Inyang et al., 2016; Inyang and Dickenson, 2015; Mahdi et al., 2018; Xiang et al., 2020). In order to scale up its usage widely available materials need to be employed; hence thorough standardised characterization of commercial biochar is needed (Mašek et al., 2018; Meyer et al., 2017). In this way the environment not only benefits through clean water, but also thanks to biochar's carbon storage potential (Morin-Crini et al., 2022; Nair et al., 2017; Oni et al., 2019). In fact, at the end of water purification through biochar, according to the adsorbed pollutants, it can also be employed in many other applications, in accordance with the key principles of circular economy and sustainable development (U.N., 2023; Hák et al., 2016; Tagliaferro et al., 2020; Wheater and Gober, 2015).

CRediT authorship contribution statement

Lorenzo Animali: Writing – review & editing, Writing – original draft, Visualization, Validation, Supervision, Resources, Methodology, Investigation, Formal analysis, Data curation, Conceptualization. **Sveva Corrado:** Writing – review & editing, Writing – original draft, Validation, Supervision, Project administration, Methodology, Investigation, Funding acquisition, Conceptualization. **Nicola Mitillo:** Writing – review & editing, Writing – original draft, Visualization, Validation, Methodology, Investigation, Formal analysis, Data curation. **Paola Tuccimei:** Writing – review & editing, Validation, Methodology, Investigation. **Mattia Bartoli:** Writing – review & editing, Validation, Methodology, Formal analysis. **Massimo Mattei:** Writing – review & editing, Project administration, Funding acquisition. **Mauro Giorcelli:** Writing – review & editing, Validation, Supervision, Project administration, Funding acquisition, Conceptualization.

Declaration of competing interest

The authors declare that they have no known competing financial interests or personal relationships that could have appeared to influence the work reported in this paper.

Acknowledgments

We are greatly thankful to Sustainable Horizons Journal Associate Editor Bing-Jie Ni, PhD and four anonymous referees for the very constructive criticism that greatly helped to improve the first version of the manuscript.

We are enormously grateful to Vito Consoli, Filippa De Martino and Silvana Rodolico of the "Direzione Ambiente Regione Lazio" for providing environmental data on Malagrotta landfill area and partially funding this research, as well as for lively discussions on environmental issues in Lazio region and Rome urban area. We also thank Luigi Iannitti of Reset SpA who kindly provided one of the biochar investigated in this research and related full production data, alongside with discussion on biochar applications.

FESEM analyses were performed at the Laboratory of Microscopy of the Department of Applied Science and Technology (DISAT) POLITO. Organic petrography at the Academic Laboratory of Basin Analysis (ALBA) of the Department of Science of Roma Tre university. FT-IR analyses at the Laboratory of FT-IR spectroscopy of the Department of Sciences of Roma Tre University. PH, Eh analyses and leaching experiments at the Geochemistry Laboratory of the Department of Sciences of Roma Tre University. XRD analyses at Department of Earth Sciences of Roma Sapienza University. Water quality analyses at C.S.A. laboratories (Gruppo C.S.A. S.p.A., Via al Torrente 22, Rimini, 47923 RN, Italy). Ion coupled plasma mass spectroscopy (ICP-MS) at the Activation Laboratories Ltd. 41 Bittern Street, Ancaster, Ontario, Canada. Fabio Bellatreccia and Luca Aldega are warmly acknowledged for providing FT-IR and XRD facilities and expertise, respectively.

Fundings: Italian Ministery of University and Research (MUR) PhD fundings (XXXVIII cycle) to L. Animali, Rome Technopole Foundation (project PNRR Rome Technopole Innovation Ecosystem – CUP F83B22000040006 to S. Corrado, N. Mitillo and M. Mattei), Direzione Ambiente Regione Lazio (Project UGOV n° 18770 818000-COMM-2024-BIOCHAR_Corrado 2023-25 to S. Corrado), PhD School in Earth Sciences to L. Animali, Project "Antropocene 2.0″ Dipartimento di Scienze-Dipartimento d'eccellenza MUR 2023 – 2027.

Supplementary materials

Supplementary material associated with this article can be found, in the online version, at doi:10.1016/j.horiz.2025.100145.

References

Adhikari, S., Moon, E., Paz-Ferreiro, J., Timms, W., 2024. Comparative analysis of biochar carbon stability methods and implications for carbon credits. Sci. Total Environ. 914, 169607. https://doi.org/10.1016/j.scitotenv.2023.169607.

Adhikari, S., Nam, H., Chakraborty, J.P., 2018. Chapter 8 - Conversion of Solid Wastes to Fuels and Chemicals Through Pyrolysis. Waste Biorefinery. Elsevier. https://doi.org/10.1016/B978-0-444-63992-9.00008-2.

Alsawy, T., Rashad, E., El-Qelish, M., Mohammed, R.H., 2022. A comprehensive review on the chemical regeneration of biochar adsorbent for sustainable wastewater treatment. NPJ. Clean. Water. 5 (1), 29. https://doi.org/10.1038/s41545-022-00172-3.

Amin, F.R., Huang, Y., He, Y., Zhang, R., Liu, G., Chen, C., 2016. Biochar applications and modern techniques for characterization. Clean. Technol. Environ. Policy. 18, 1457–1473. https://doi.org/10.1007/s10098-016-1218-8.

APAT, 2003. Agenzia per la protezione dell'ambiente (APAT) e per i servizi tecnici and Istituto di Ricerca sulle Acque - Consiglio Nazionale delle Ricerche (IRSA-CNR). Metodi Analitici per le Acque. https://www.irsa.cnr.it/wp/wp-content/uploads/2022/04/Vol1_Sez_1000_Indice_ParteGenerale.pdf.

ARPALAZIO, 2020. Agenzia Regionale Protezione Ambientale del Lazio. Anagrafica delle stazioni di monitoraggio dei corsi d'acqua aggiornata in base alla delibera della Giunta della Regione Lazio n. 77 del 02 marzo 2020. https://www.arpalazio.it/documents/20124/53499/anagraficaCorsiAcqua_aggiornata_77.pdf.

Baderna, D., Maggioni, S., Boriani, E., Gemma, S., Molteni, M., Lombardo, A., Colombo, A., Bordonali, S., Rotella, G., Lodi, M., Benfenati, E., 2011. A combined approach to investigate the toxicity of an industrial landfill's leachate: chemical analyses, risk assessment and in vitro assays. Environ. Res. 111, 603–613. https://doi.org/10.1016/j.envres.2011.01.015.

Barbieri, M., Sappa, G., Vitale, S., Parisse, B., Battistel, M., 2014. Soil control of trace metals concentrations in landfills: a case study of the largest landfill in Europe, Malagrotta, Rome. J. Geochem. Explor. 143, 146–154. https://doi.org/10.1016/j.gexplo.2014.04.001.

Bayar, J., Ali, N., Dong, Y., Ahmad, U., Anjum, M.M., Khan, G.R., Zaib, M., Jalal, A., Ali, R., Ali, L., 2024. Biochar-based adsorption for heavy metal removal in water: a sustainable and cost-effective approach. Environ. Geochem. Health 46 (11), 428. https://doi.org/10.1007/s10653-024-02214-w.

Brassard, P., Godbout, S., Raghavan, V., 2017. Pyrolysis in auger reactors for biochar and bio-oil production: a review. Biosyst. Eng. 161, 80–92. https://doi.org/10.1016/j.biosystemseng.2017.06.020.

Bustin, R.M., Cameron, A.R., Grieve, D.A., Kalkreuth, W.D., 1985. Coal petrology: Its principles, methods, and Applications. Canada.

Caricchi, C., Corrado, S., Di Paolo, L., Aldega, L., Grigo, D., 2016. Thermal maturity of Silurian deposits in the Baltic Syneclise (on-shore Polish Baltic Basin): contribution

to unconventional resources assessment. Italian J. Geosci. 135, 383–393. https://doi.org/10.3301/IJG.2015.16.
Castiglioni, M., Rivoira, L., Ingrando, I., Meucci, L., Binetti, R., Fungi, M., El-Ghadraoui, A., Bakari, Z., Del Bubba, M., Bruzzoniti, M.C., 2022. Biochars intended for water filtration: a comparative study with activated carbons of their physicochemical properties and removal efficiency towards neutral and anionic organic pollutants. Chemosphere 288, 132538. https://doi.org/10.1016/j.chemosphere.2021.132538.
CEN, 2004. European Committee for Standardization. Standard EN 12902:2004. Products used for treatment of water intended for human consumption - inorganic supporting and filtering materials - methods of test. https://standards.iteh.ai/catalog/standards/cen/972e462c-c07c-4a27-a11f-0f9bcf5f5507/en-12902-2004?srsltid=AfmBOordHIrTK0xKrjbSRAMmYTS-1wgTjFWn0a7mGYafLRuj5tnGiZps.
CEN, 2009a. European Committee for Standardization. Standard EN 12903:2009. Products used for the treatment of water intended for human consumption - powdered activated carbon. https://standards.cencenelec.eu/dyn/www/f?p=CEN:110:0::::FSP_PROJECT,FSP_ORG_ID:30424,6145&cs=124B38EAC5C46B273488249582DC4F853.
CEN, 2009b European Committee for Standardization. Standard EN 12915-1:2009. Products used for the treatment of water intended for human consumption - granular activated carbon - part 1: virgin granular activated carbon. https://standards.cencenelec.eu/dyn/www/f?p=CEN:110:0::::FSP_PROJECT,FSP_ORG_ID:30426,6145&cs=146F11CEBF32E14FB03B182319D58188C.
CEN, 2009c. European Committee for Standardization. Standard EN 12915-2:2009. Products used for the treatment of water intended for human consumption - granular activated carbon - part 2: reactivated granular activated carbon. https://standards.cencenelec.eu/dyn/www/f?p=CEN:110:0::::FSP_PROJECT,FSP_ORG_ID:30427,6145&cs=18DAD99F2B4800D56D436408E556DB087.
Chen, B., Zhou, D., Zhu, L., 2008. Transitional adsorption and partition of nonpolar and polar aromatic contaminants by biochars of pine needles with different pyrolytic temperatures. Environ. Sci. Technol. 42, 5137–5143. https://doi.org/10.1021/es8002684.
Chen, Y., Mastalerz, M., Schimmelmann, A., 2012. Characterization of chemical functional groups in macerals across different coal ranks via micro-FTIR spectroscopy. Int. J. Coal. Geol. 104, 22–33. https://doi.org/10.1016/j.coal.2012.09.001.
Chen, W., Meng, J., Han, X., Lan, Y., Zhang, W., 2019. Past, present, and future of biochar. Biochar. 1, 75–87. https://doi.org/10.1007/s42773-019-00008-3.
Chen, W.-H., Hoang, A.T., Nižetić, S., Pandey, A., Cheng, C.K., Luque, R., Ong, H.C., Thomas, S., Nguyen, X.P., 2022. Biomass-derived biochar: from production to application in removing heavy metal-contaminated water. Process Safety Environ. Protect. 160, 704–733. https://doi.org/10.1016/j.psep.2022.02.061.
Clemente, J.S., Beauchemin, S., Thibault, Y., Mackinnon, T., Smith, D., 2018. Differentiating inorganics in biochars produced at commercial scale using principal component analysis. ACS. Omega 3, 6931–6944. https://doi.org/10.1021/acsomega.8b00523.
Dai, L., Lu, Q., Zhou, H., Shen, F., Liu, Z., Zhu, W., Huang, H., 2021. Tuning oxygenated functional groups on biochar for water pollution control: a critical review. J. Hazard. Mater. 420, 126547. https://doi.org/10.1016/j.jhazmat.2021.126547.
Daniele, L., Fabiani, M., 2020. L'imputabilità dei costi di gestione delle discariche dismesse secondo una recente sentenza della Corte di giustizia: il caso "Malagrotta". EUROJUS, Fascicolo n. 4 - 2020. https://art.torvergata.it/bitstream/2108/261901/1/Il%20caso%20Malagrotta%20Eurojus%20Daniele-Fabiani.pdf.
Das, O., Sarmah, A.K., 2015. The love–hate relationship of pyrolysis biochar and water: a perspective. Sci. Total Environ. 512-513, 682–685. https://doi.org/10.1016/j.scitotenv.2015.01.061.
Di Paolo, L., Aldega, L., Corrado, S., Mastalerz, M., 2012. Maximum burial and unroofing of Mt. Judica recess area in Sicily: implication for the apenninic–Maghrebian wedge dynamics. Tectonophysics. 530, 193–207. https://doi.org/10.1016/j.tecto.2011.12.020.
Dinh, V.-P., Nguyen, D.-K., Luu, T.-T., Nguyen, Q.-H., Tuyen, L.A., Phong, D.D., Kiet, H.A.T., Ho, T.-H., Nguyen, T.T.P., Xuan, T.D., Hue, P.T., Hue, N.T.N., 2022. Adsorption of Pb(II) from aqueous solution by pomelo fruit peel-derived biochar. Mater. Chem. Phys. 285, 126105. https://doi.org/10.1016/j.matchemphys.2022.126105.
EBC, 2023. Guidelines of the European Biochar Certificate - version 10.3. https://www.european-biochar.org/en (accessed 18 December 2024).
EPA, 1994. U.S. Environmental Protection Agency (EPA). Method 200.7 - determination of metals and trace elements in water and wastes by inductively coupled plasma - atomic emission spectrometry. Revision 4.4. https://www.epa.gov/sites/default/files/2015-06/documents/epa-200.7.pdf.
EPA, 2004. U.S. Environmental Protection Agency (EPA). Method 9010C - total and amenable cyanide: distillation. Revision 3. https://www.epa.gov/sites/default/files/2015-12/documents/9010c.pdf.
EPA, 2014. U.S. Environmental Protection Agency (EPA). Method 9014 - cyanide in waters and extracts using titrimetric and manual spectrophotometric procedures. Revision 1. https://www.epa.gov/sites/default/files/2015-12/documents/9014.pdf.
ERAS, 2013. Epidemiologia rifiuti Ambiente e Salute (ERAS), Regione Lazio. Valutazione epidemiologica dello stato di salute della popolazione residente nell'area di Malagrotta a Roma. Programma ERASLazio – Rapporto Salute. All. 2. https://www.eraslazio.it/impianti/malagrotta-complesso-roma (accessed 18 December 2024).
EU, 2000. Directive 2000/60/EC of the European Parliament and of the Council of 23 October 2000. http://data.europa.eu/eli/dir/2000/60/oj (accessed 16 January 2024).
EU, 2006. Regulation (EC) No 1907/2006 of the European Parliament and of the Council of 18 December 2006. Official J. Eur. Union. http://data.europa.eu/eli/reg/2006/1907/oj. accessed 16 January 2024.
EU, 2019. Regulation (EU) 2019/1009 of the European Parliament and of the Council of 5 June 2019. Official J. Eur. Union. http://data.europa.eu/eli/reg/2019/1009/oj. accessed 16 January 2024.
Filibeck, G., Petrella, P., Cornelini, P., 2016. All ecosystems look messy, but some more so than others: a case-study on the management and acceptance of Mediterranean urban grasslands. Urban. For. Urban. Green. 15, 32–39. https://doi.org/10.1016/j.ufug.2015.11.005.
Goñi-Urtiaga, A., Courtier-Murias, D., Picca, G., Valentín, J.L., Plaza, C., Panettieri, M., 2022. Response of water-biochar interactions to physical and biochemical aging. Chemosphere 307, 136071. https://doi.org/10.1016/j.chemosphere.2022.136071.
Hák, T., Janoušková, S., Moldan, B., 2016. Sustainable Development Goals: a need for relevant indicators. Ecol. Indic. 60, 565–573. https://doi.org/10.1016/j.ecolind.2015.08.003.
Hassan, M., Liu, Y., Naidu, R., Parikh, S.J., Du, J., Qi, F., Willett, I.R., 2020. Influences of feedstock sources and pyrolysis temperature on the properties of biochar and functionality as adsorbents: a meta-analysis. Sci. Total Environ. 744, 140714. https://doi.org/10.1016/j.scitotenv.2020.140714.
Hou, J., Huang, L., Yang, Z., Zhao, Y., Deng, C., Chen, Y., Li, X., 2016. Adsorption of ammonium on biochar prepared from giant reed. Environ. Sci. Pollut. Res. 23, 19107–19115. https://doi.org/10.1007/s11356-016-7084-4.
Huang, Q., Song, S., Chen, Z., Hu, B., Chen, J., Wang, X., 2019. Biochar-based materials and their applications in removal of organic contaminants from wastewater: state-of-the-art review. Biochar. 1, 45–73. https://doi.org/10.1007/s42773-019-00006-5.
Iamsaard, K., Weng, C.-H., Yen, L.-T., Tzeng, J.-H., Poonpakdee, C., Lin, Y.-T., 2022. Adsorption of metal on pineapple leaf biochar: key affecting factors, mechanism identification, and regeneration evaluation. Bioresour. Technol. 344, 126131. https://doi.org/10.1016/j.biortech.2021.126131.
Ilić, M., Haegel, F.-H., Lolić, A., Nedić, Z., Tosti, T., Ignjatović, I.S., Linden, A., Jablonowski, N.D., Hartmann, H., 2022. Surface functional groups and degree of carbonization of selected chars from different processes and feedstock. PLoS. One 17, e0277365. https://doi.org/10.1371/journal.pone.0277365.
Inyang, M., Dickenson, E., 2015. The potential role of biochar in the removal of organic and microbial contaminants from potable and reuse water: a review. Chemosphere 134, 232–240. https://doi.org/10.1016/j.chemosphere.2015.03.072.
Inyang, M.I., Gao, B., Yao, Y., Xue, Y., Zimmerman, A., Mosa, A., Pullammanappallil, P., Ok, Y.S., Cao, X., 2016. A review of biochar as a low-cost adsorbent for aqueous heavy metal removal. Crit. Rev. Environ. Sci. Technol. 46, 406–433. https://doi.org/10.1080/10643389.2015.1096880.
Ippolito, J.A., Cui, L., Kammann, C., Wrage-Mönnig, N., Estavillo, J.M., Fuertes-Mendizabal, T., Cayuela, M.L., Sigua, G., Novak, J., Spokas, K., Borchard, N., 2020. Feedstock choice, pyrolysis temperature and type influence biochar characteristics: a comprehensive metadata analysis review. Biochar. 2, 421–438. https://doi.org/10.1007/s42773-020-00067-x.
ISO, 2007. International Organization for Standardization, ISO 10304-1:2007, water quality - determination of dissolved anions by liquid chromatography of ions. https://www.iso.org/standard/46004.html (accessed 18 December 2024).
ISO, 2012. International Organization for Standardization, ISO 12846:2012, water quality - determination of mercury - method using atomic absorption spectrometry (AAS) with and without enrichment. https://www.iso.org/standard/51964.html (accessed 18 December 2024).
ISO, 2023. International Organization for Standardization, ISO 17294-2:2023, water quality - application of inductively coupled plasma mass spectrometry (ICP-MS). https://www.iso.org/standard/82245.html (accessed 18 December 2024).
Jones, E.R., Bierkens, M.F., Wanders, N., Sutanudjaja, E.H., van Beek, L.P., van Vliet, M.T., 2022. Current wastewater treatment targets are insufficient to protect surface water quality. Commun. Earth. Environ. 3 (1), 221. https://doi.org/10.1038/s43247-022-00554-y.
Janu, R., Mrlik, V., Ribitsch, D., Hofman, J., Sedláček, P., Bielská, L., Soja, G., 2021. Biochar surface functional groups as affected by biomass feedstock, biochar composition and pyrolysis temperature. Carbon Res. Convers. 4, 36–46. https://doi.org/10.1016/j.crcon.2021.01.003.
Joshi, K., Navalgund, L., Shet, V.B., 2022. Water pollution from construction industry: an introduction. In: Malik, J.A., Marathe, S. (Eds.), Ecological and Health Effects of Building Materials. Springer, Cham. https://doi.org/10.1007/978-3-030-76073-1_13.
Kamali, M., Appels, L., Kwon, E.E., Aminabhavi, T.M., Dewil, R., 2021. Biochar in water and wastewater treatment-a sustainability assessment. Chem. Eng. J. 420, 129946. https://doi.org/10.1016/j.cej.2021.129946.
Keiluweit, M., Nico, P.S., Johnson, M.G., Kleber, M., 2010. Dynamic molecular structure of plant biomass-derived black carbon (Biochar). Environ. Sci. Technol. 44, 1247–1253. https://doi.org/10.1021/es9031419.
Kersten, S., Garcia-Perez, M., 2013. Recent developments in fast pyrolysis of ligno-cellulosic materials. Curr. Opin. Biotechnol. 24, 414–420. https://doi.org/10.1016/j.copbio.2013.04.003.
Kim, J.-Y., Oh, S., Park, Y.-K., 2020. Overview of biochar production from preservative-treated wood with detailed analysis of biochar characteristics, heavy metals behaviors, and their ecotoxicity. J. Hazard. Mater. 384, 121356. https://doi.org/10.1016/j.jhazmat.2019.121356.
Kwon, E.E., Kim, S., Lee, J., 2019. Pyrolysis of waste feedstocks in CO_2 for effective energy recovery and waste treatment. J. CO2 Utiliz. 31, 173–180. https://doi.org/10.1016/j.jcou.2019.03.015.
Lehmann, J., Cowie, A., Masiello, C.A., Kammann, C., Woolf, D., Amonette, J.E., Cayuela, M.L., Camps-Arbestain, M., Whitman, T., 2021. Biochar in climate change mitigation. Nat. Geosci. 14, 883–892. https://doi.org/10.1038/s41561-021-00852-8.

Leng, L., Huang, H., Li, H., Li, J., Zhou, W., 2019. Biochar stability assessment methods: a review. Sci. Total Environ. 647, 210–222. https://doi.org/10.1016/j.scitotenv.2018.07.402.

Lester, E., Alvarez, D., Borrego, A.G., Valentim, B., Flores, D., Clift, D.A., Rosenberg, P., Kwiecinska, B., Barranco, R., Petersen, H.I., Mastalerz, M., Milenkova, K.S., Panaitescu, C., Marques, M.M., Thompson, A., Watts, D., Hanson, S., Predeanu, G., Misz, M., Wu, T., 2010. The procedure used to develop a coal char classification - commission III combustion working group of the international committee for coal and organic petrology. Int. J. Coal. Geol. 81 (4), 333–342. https://doi.org/10.1016/j.coal.2009.10.015.

Li, M., Liu, Q., Guo, L., Zhang, Y., Lou, Z., Wang, Y., Qian, G., 2013. Cu(II) removal from aqueous solution by Spartina alterniflora derived biochar. Bioresour. Technol. 141, 83–88. https://doi.org/10.1016/j.biortech.2012.12.096.

Lian, W., Li, H., Yang, J., Joseph, S., Bian, R., Liu, X., Zheng, J., Drosos, M., Zhang, X., Li, L., Shan, S., Pan, G., 2021. Influence of pyrolysis temperature on the cadmium and lead removal behavior of biochar derived from oyster shell waste. Bioresour. Technol. Rep. 15, 100709. https://doi.org/10.1016/j.biteb.2021.100709.

Lin, L., Yang, H., Xu, X., 2022. Effects of water pollution on Human health and disease heterogeneity: a review. Front. Environ. Sci. 10. https://doi.org/10.3389/fenvs.2022.880246.

Lis, G.P., Mastalerz, M., Schimmelmann, A., Lewan, M.D., Stankiewicz, B.A., 2005. FTIR absorption indices for thermal maturity in comparison with vitrinite reflectance R_0 in type-II kerogens from Devonian black shales. Org. Geochem. 36, 1533–1552. https://doi.org/10.1016/j.orggeochem.2005.07.001.

Liu, Z., Tian, D., Shen, F., Long, L., Zhang, Y., Yang, G., Zeng, Y., Zhang, J., He, J., Zhu, Y., Deng, S., 2019. Elucidating dominant factors of PO_4^{3-}, Cd^{2+} and nitrobenzene removal by biochar: a comparative investigation based on distinguishable biochars. Chin. Chem. Lett. 30, 2221–2224. https://doi.org/10.1016/j.cclet.2019.04.016.

A. L. Ltd., 2024a. Activation Laboratories Ltd. (Actlabs), “core, rocks, drill cuttings - code RX4”. https://actlabs.com/geochemistry/sample-preparation/core-rocks-drill-cuttings/(accessed 18 December 2024).

A. L. Ltd., 2024b Activation Laboratories Ltd. (Actlabs), “Ultratrace 4 - Near Total digestion - ICP and ICP-MS”. https://actlabs.com/geochemistry/exploration-geochemistry/4-acid-near-total-digestion/#81f275af7e5816bc4/(accessed 18 December 2024).

Mahdi, Z., Yu, Q.J., El Hanandeh, A., 2018. Removal of lead(II) from aqueous solution using date seed-derived biochar: batch and column studies. Appl. Water. Sci. 8, 181. https://doi.org/10.1007/s13201-018-0829-0.

Mašek, O., Buss, W., Sohi, S., 2018. Standard biochar materials. Environ. Sci. Technol. 52, 9543–9544. https://doi.org/10.1021/acs.est.8b04053.

Mastalerz, M., Drobniak, A., Briggs, D., Bradburn, J., 2023. Variations in microscopic properties of biomass char: implications for biochar characterization. Int. J. Coal. Geol. 271, 104235. https://doi.org/10.1016/j.coal.2023.104235.

Md Salim, R., Asik, J., Sarjadi, M.S., 2021. Chemical functional groups of extractives, cellulose and lignin extracted from native Leucaena leucocephala bark. Wood Sci. Technol. 55, 295–313. https://doi.org/10.1007/s00226-020-01258-2.

Meyer, S., Genesio, L., Vogel, I., Schmidt, H.-P., Soja, G., Someus, E., Shackley, S., Verheijen, F.G.A., Glaser, B., 2017. Biochar standardization and legislation harmonization. J. Environ. Eng. Landscape Manag. 25, 175–191. https://doi.org/10.3846/16486897.2016.1254640.

D. Lgs, 2010. Presidenza del Consiglio dei Ministri, Decreto Legislativo 29 aprile 2010, n. 75. Gazzetta Ufficiale della Repubblica Italiana. https://www.normattiva.it/uri-res/N2Ls?urn:nir:stato:decreto.legislativo:2010-04-29;75/. accessed 18 December 2024.

D.Lgs. n.18, 2023. Presidenza del Consiglio dei Ministri, Decreto Legislativo 23 febbraio 2023, n. 18. Gazzetta Ufficiale della Repubblica Italiana. https://www.normattiva.it/uri-res/N2Ls?urn:nir:stato:decreto.legislativo:2023;018/. (accessed 18 December 2024).

Mohan, D., Pittman, C.U., Bricka, M., Smith, F., Yancey, B., Mohammad, J., Steele, P.H., Alexandre-Franco, M.F., Gómez-Serrano, V., Gong, H., 2007. Sorption of arsenic, cadmium, and lead by chars produced from fast pyrolysis of wood and bark during bio-oil production. J. Colloid. Interface Sci. 310, 57–73. https://doi.org/10.1016/j.jcis.2007.01.020.

Morga, R., 2010. Chemical structure of semifusinite and fusinite of steam and coking coal from the Upper Silesian Coal Basin (Poland) and its changes during heating as inferred from micro-FTIR analysis. Int. J. Coal. Geol., 84, 1–15. https://doi.org/10.1016/j.coal.2010.07.003.

Morga, R., 2011. Changes of semifusinite and fusinite surface roughness during heat treatment determined by atomic force microscopy. Int. J. Coal. Geol. 88, 218–226. https://doi.org/10.1016/j.coal.2011.10.009.

Morin-Crini, N., Lichtfouse, E., Liu, G., Balaram, V., Ribeiro, A.R.L., Lu, Z., Stock, F., Carmona, E., Teixeira, M.R., Picos-Corrales, L.A., Moreno-Piraján, J.C., Giraldo, L., Li, C., Pandey, A., Hocquet, D., Torri, G., Crini, G., 2022. Worldwide cases of water pollution by emerging contaminants: a review. Environ. Chem. Lett. 20, 2311–2338. https://doi.org/10.1007/s10311-022-01447-4.

Moyo, M., Lindiwe, S.T., Sebata, E., Nyamunda, B.C., Guyo, U., 2016. Equilibrium, kinetic, and thermodynamic studies on biosorption of Cd(II) from aqueous solution by biochar. Res. Chem. Intermed. 42, 1349–1362. https://doi.org/10.1007/s11164-015-2089-z.

Nair, V.D., Nair, P.K.R., Dari, B., Freitas, A.M., Chatterjee, N., Pinheiro, F.M., 2017. Biochar in the agroecosystem–climate-change–sustainability nexus. Front. Plant Sci. 8. https://doi.org/10.3389/fpls.2017.02051.

Oleszczuk, P., Ćwikła-Bundyra, W., Bogusz, A., Skwarek, E., Ok, Y.S., 2016. Characterization of nanoparticles of biochars from different biomass. J. Anal. Appl. Pyrolysis. 121, 165–172. https://doi.org/10.1016/j.jaap.2016.07.017.

Oni, B.A., Oziegbe, O., Olawole, O.O., 2019. Significance of biochar application to the environment and economy. Ann. Agricult. Sci. 64, 222–236. https://doi.org/10.1016/j.aoas.2019.12.006.

Painter, P., Coleman, M., Snyder, R., Mahajan, O., Komatsu, M., Walker, P., 1981. Low temperature air oxidation of caking coals: fourier transform infrared studies. Appl. Spectrosc. 35, 106–110. https://doi.org/10.1366/000370281473184.

Petersen, H.I., Rosenberg, P., Nytoft, H.P., 2008. Oxygen groups in coals and alginite-rich kerogen revisited. Int. J. Coal. Geol. 74, 93–113. https://doi.org/10.1016/j.coal.2007.11.007.

Phan, V.T.H., Quirico, E., Beck, P., Le Brech, Y., Jovanovic, L., Le Guillou, C., Bernard, S., Bonal, L., Carrasco, N., Gautier, T., 2021. Infrared spectroscopy quantification of functional carbon groups in kerogens and coals: a calibration procedure. Spectrochim. Acta Part A: Mol. Biomol. Spectrosc. 259, 119853. https://doi.org/10.1016/j.saa.2021.119853.

Pourhashem, G., Hung, S.Y., Medlock, K.B., Masiello, C.A., 2019. Policy support for biochar: review and recommendations. GCB Bioenergy 11, 364–380. https://doi.org/10.1111/gcbb.12582.

Rajput, V., Saini, I., Parmar, S., Pundir, V., Kumar, V., Kumar, V., Naik, B., Rustagi, S., 2024. Biochar production methods and their transformative potential for environmental remediation. Discover Appl. Sci. 6, 408. https://doi.org/10.1007/s42452-024-06125-4.

Reza, M.S., Afroze, S., Bakar, M.S., Saidur, R., Aslfattahi, N., Taweekun, J., Azad, A.K., 2020. Biochar characterization of invasive Pennisetum purpureum grass: effect of pyrolysis temperature. Biochar. 2, 239–251. https://doi.org/10.1007/s42773-020-00048-0.

Sakhiya, A.K., Anand, A., Kaushal, P., 2020. Production, activation, and applications of biochar in recent times. Biochar. 2, 253–285. https://doi.org/10.1007/s42773-020-00047-1.

Schwarzenbach, R.P., Egli, T., Hofstetter, T.B., Von Gunten, U., Wehrli, B., 2010. Global water pollution and Human health. Annu Rev. Environ. Resour. 35, 109–136. https://doi.org/10.1146/annurev-environ-100809-125342.

Singh, B., Camps-Arbestain, M., Lehmann, J., 2017. Biochar, a Guide to Analytical Methods. CSIRO Publishing.

Singh, B., Fang, Y., Johnston, C., 2016. A fourier-transform infrared study of biochar aging in soils. Soil Sci. Soc. Am. J. 80, 613–622. https://doi.org/10.2136/sssaj2015.11.0414.

SIRA, 2024. Sistema Informativo Regionale Ambientale del Lazio (SIRA), Valutazioni - Carta dei Giudizi. Water Framework Directive, Decreto Legislativo 152/2006 all.1 - corpi idrici fluviali. https://arpasira.regione.lazio.it/sira/carta-giudizi/acqua (accessed 18 December 2024).

Sorrenti, G., Masiello, C.A., Dugan, B., Toselli, M., 2016. Biochar physico-chemical properties as affected by environmental exposure. Sci. Total Environ. 563-564, 237–246. https://doi.org/10.1016/j.scitotenv.2016.03.245.

Spokas, K.A., Novak, J.M., Masiello, C.A., Johnson, M.G., Colosky, E.C., Ippolito, J.A., Trigo, C., 2014. Physical disintegration of Biochar: an overlooked process. Environ. Sci. Technol. Lett. 1, 326–332. https://doi.org/10.1021/ez500199t.

Strokal, M., Bai, Z., Franssen, W., Hofstra, N., Koelmans, A.A., Ludwig, F., Ma, L., Van Puijenbroek, P., Spanier, J.E., Vermeulen, L.C., Van Vliet, M.T.H., Van Wijnen, J., Kroeze, C., 2021. Urbanization: an increasing source of multiple pollutants to rivers in the 21st century. npj Urban Sustainability 1, 24. https://doi.org/10.1038/s42949-021-00026-w.

Sun, T., Pei, P., Sun, Y., Xu, Y., Jia, H., 2022. Performance and mechanism of As(III/V) removal from aqueous solution by novel positively charged animal-derived biochar. Sep. Purif. Technol. 290, 120836. https://doi.org/10.1016/j.seppur.2022.120836.

Tagliaferro, A., Rosso, C., Giorcelli, M., 2020. Biochar. Emerging applications. IOP Publishing. https://doi.org/10.1088/978-0-7503-2660-5.

Tan, X.-F., Liu, S.-B., Liu, Y.-G., Gu, Y.-L., Zeng, G.-M., Hu, X.-J., Wang, X., Liu, S.-H., Jiang, L.-H., 2017. Biochar as potential sustainable precursors for activated carbon production: multiple applications in environmental protection and energy storage. Bioresour. Technol. 227, 359–372. https://doi.org/10.1016/j.biortech.2016.12.083.

Tomczyk, A., Sokołowska, Z., Boguta, P., 2020. Biochar physicochemical properties: pyrolysis temperature and feedstock kind effects. Rev. Environ. Sci. Bio/Technol. 19, 191–215. https://doi.org/10.1007/s11157-020-09523-3.

UNESCO, 2021. World Water Assessment Programme. The United Nations world water development report 2021: valuing water. https://unesdoc.unesco.org/ark:/48223/pf0000375724 (accessed 18 December 2024).

U.N., 2023. United Nations - the sustainable development goals - report 2023: special edition. Towards a Rescue Plan for People and Planet. https://sdgs.un.org/sites/default/files/2023-07/The-Sustainable-Development-Goals-Report-2023_0.pdf.

Van Hien, N., Valsami-Jones, E., Vinh, N.C., Phu, T.T., Tam, N.T.T., Lynch, I., 2020. Effectiveness of different biochar in aqueous zinc removal: correlation with physicochemical characteristics. Bioresour. Technol. Rep. 11, 100466. https://doi.org/10.1016/j.biteb.2020.100466.

Wang, J., Wang, S., 2019. Preparation, modification and environmental application of biochar: a review. J. Clean. Prod. 227, 1002–1022. https://doi.org/10.1016/j.jclepro.2019.04.282.

Wang, X., Guo, Z., Hu, Z., Zhang, J., 2020. Recent advances in biochar application for water and wastewater treatment: a review. PeerJ, Life Environ. https://doi.org/10.7717/peerj.9164.

Weber, K., Quicker, P., 2018. Properties of biochar. Fuel 217, 240–261. https://doi.org/10.1016/j.fuel.2017.12.054.

Wei, D., Li, B., Huang, H., Luo, L., Zhang, J., Yang, Y., Guo, J., Tang, L., Zeng, G., Zhou, Y., 2018. Biochar-based functional materials in the purification of agricultural wastewater: fabrication, application and future research needs. Chemosphere 197, 165–180. https://doi.org/10.1016/j.chemosphere.2017.12.193.

Werdin, J., Fletcher, T.D., Rayner, J.P., Williams, N.S.G., Farrell, C., 2020. Biochar made from low density wood has greater plant available water than biochar made from high density wood. Sci. Total Environ. 705, 135856. https://doi.org/10.1016/j.scitotenv.2019.135856.

Wheater, H.S., Gober, P., 2015. Water security and the science agenda. Water. Resour. Res. 51, 5406–5424. https://doi.org/10.1002/2015WR016892.

Xiang, W., Zhang, X., Chen, J., Zou, W., He, F., Hu, X., Tsang, D.C.W., Ok, Y.S., Gao, B., 2020. Biochar technology in wastewater treatment: a critical review. Chemosphere 252, 126539. https://doi.org/10.1016/j.chemosphere.2020.126539.

Xiao, X., Chen, B., Chen, Z., Zhu, L., Schnoor, J.L., 2018. Insight into multiple and multilevel structures of biochars and their potential environmental applications: a critical review. Environ. Sci. Technol. 52, 5027–5047. https://doi.org/10.1021/acs.est.7b06487.

Yargicoglu, E.N., Sadasivam, B.Y., Reddy, K.R., Spokas, K., 2015. Physical and chemical characterization of waste wood derived biochars. Waste Manag. 36, 256–268. https://doi.org/10.1016/j.wasman.2014.10.029.

Yu, S., Zhang, W., Dong, X., Wang, F., Yang, W., Liu, C., Chen, D., 2024. A review on recent advances of biochar from agricultural and forestry wastes: preparation, modification and applications in wastewater treatment. J. Environ. Chem. Eng. 12 (1), 111638. https://doi.org/10.1016/j.jece.2023.111638.

Zamora-Ledezma, C., Negrete-Bolagay, D., Figueroa, F., Zamora-Ledezma, E., Ni, M., Alexis, F., Guerrero, V.H., 2021. Heavy metal water pollution: a fresh look about hazards, novel and conventional remediation methods. Environ. Technol. Innov. 22, 101504. https://doi.org/10.1016/j.eti.2021.101504.

Zhang, G., Liu, N., Luo, Y., Zhang, H., Su, L., Oh, K., Cheng, H., 2020. Efficient removal of Cu (II), Zn (II), and Cd (II) from aqueous solutions by a mineral-rich biochar derived from a spent mushroom (Agaricus bisporus) substrate. Materials. (Basel) 14, 35. https://doi.org/10.3390/ma14010035.

Zhang, Y., Liu, N., Liu, P., Liu, Y., Lei, Y., 2023a. Molecular-level investigation on removal mechanisms of aqueous hexavalent chromium by pine needle biochar. Arab. J. Chem. 16 (8), 104966. https://doi.org/10.1016/j.arabjc.2023.104966.

Zhang, Y., Zhang, L., Han, C., Ren, Y., Ji, Y., Ge, Y., Li, Z., He, J., 2023b. Preparation, characteristics and mechanisms of Cd (II) adsorption from aqueous solution by mango kernel-derived biochar. Biomass. Conv. Bioref. 13, 393–407. https://doi.org/10.1007/s13399-022-03050-7.

Zhao, C., Wang, B., Theng, B.K.G., Wu, P., Liu, F., Wang, S., Lee, X., Chen, M., Li, L., Zhang, X., 2021. Formation and mechanisms of nano-metal oxide-biochar composites for pollutants removal: a review. Sci. Total Environ. 767, 145305. https://doi.org/10.1016/j.scitotenv.2021.145305.

Zhao, L., Cao, X., Zheng, W., Wang, Q., Yang, F., 2015. Endogenous minerals have influences on surface electrochemistry and ion exchange properties of biochar. Chemosphere 136, 133–139. https://doi.org/10.1016/j.chemosphere.2015.04.053.

Zheng, H., Wang, Z., Deng, X., Zhao, J., Luo, Y., Novak, J., Herbert, S., Xing, B., 2013. Characteristics and nutrient values of biochars produced from giant reed at different temperatures. Bioresour. Technol. 130, 463–471. https://doi.org/10.1016/j.biortech.2012.12.044.

Lorenzo Animali – Ph.D. student in Earth Sciences at the Department of Science at Roma Tre university with a master's degree in Geoenvironmental Resources and Risk. He is currently carrying out research regarding characterization and use of biochar for climate change mitigation.

Sveva Corrado – Full professor at the Department of Science at Roma Tre university, Ph.D. in Earth Sciences. Expertise in structural geology with specific interest in thermal and tectonic evolution of fold and thrust belts and sedimentary basins for energy E&P. Winner of the "Secondo Franchi Award".

Nicola Mitillo – Postdoctoral fellow at the Department of Science at Roma Tre university, Ph.D. in Earth Sciences. Expertise in evaluation of carbon storage potential in carbonate reservoirs and spectroscopy of organic matter.

Paola Tuccimei – Associate professor at the Department of Science at Roma Tre university, Ph.D. in Earth Sciences. Her research concerns Environmental geochemistry with a focus on isotopic studies for environmental, paleoenvironmental, paleoclimatic and volcanological applications.

Mattia Bartoli – Postdoctoral fellow at Center for Sustainable Future Technologies (CSFT) at Politecnico di Torino, Ph.D. in Chemical Science. Expert in carbon and bismuth-based materials and composites for environmental remediation and biological applications, metal coordinated polymers and copolymers and microwave pyrolysis of biomass. Sustainability board member at National Interuniversity Consortium for Materials Science and Technology (INSTM).

Massimo Mattei – Full professor at the Department of Science at Roma Tre university, Ph.D. in Earth Sciences. His studies encompass paleomagnetism, paleogeographic reconstructions, also trough the usage of isotopic techniques. Simultaneously, its career has also been devoted to outreach with a keen interest to sustainable development.

Mauro Giorcelli - Associate professor at the Department of Applied Science and Technology (DISAT) at Politecnico di Torino, Ph.D. in Electronics Physics Nanotechnology. His main field of expertise is on carbon materials, spanning from their characterization to application in composites. Internationally recognized expert in innovative biochar applications. Italian biochar association (ICHAR) executive member and part of the European Biochar Industry consortium (EBI) scientific council.